not sent out as new prob.
784

Letter of Intent for the BCD

A Bottom Collider Detector for the Fermilab Tevatron

H. Castro, B. Gomez, F. Rivera, J.-C. Sanabria, *Universidad de los Andes*
P. Yager, *University of California, Davis*
E. Barsotti, M. Bowden, S. Childress, P. Lebrun, J. Morfin, L.A. Roberts,
R. Stefanski, L. Stutte, C. Swoboda *Fermilab*
P. Avery, J. Yelton, *University of Florida*
K. Lau, *University of Houston*
R. Burnstein, H. Rubin, *Illinois Institute of Technology*
E. McCliment, Y. Onel, *University of Iowa*
G. Alverson, W. Faissler, D. Garelick, M. Glaubman, I. Leedom, S. Reucroft,
D. Kaplan, *Northeastern University*
S. E. Willis, *Northern Illinois University*
S. Fredricksen, N. W. Reay, C. Rush, R. A. Sidwell, N. Stanton,
Ohio State University
G. R. Kalbfleisch, P. Skubic, J. Snow, *University of Oklahoma*
N. S. Lockyer, *University of Pennsylvania*
D. Judd, D. Wagoner, *Prairie View A&M University*
K. T. McDonald, *Princeton University*
A. Lopez, *Universidad de Puerto Rico*
B. Hoeneisen, *Universidad San Francisco de Quito*
S. Dhawan, P. E. Karchin, W. Ross, A. J. Slaughter, *Yale University*

(October 7, 1988)

Abstract

A dedicated B physics experiment is proposed for the Fermilab Tevatron p-$\bar{p}$ Collider. The goal is to study the full range of physics associated with 10^{10} produced $B\bar{B}$ pairs per year. This corresponds to a run of 10^7 sec at an average luminosity of 10^{31} cm^{-2}sec^{-1}, with a $\sigma_{B\bar{B}} \sim 45$ μbarns and a ratio of 1 $B\bar{B}$ pair/1000 inelastic events. Since B decay products have typical P_T's of only a few GeV/c, this physics is not accessible to a conventional p-$\bar{p}$ detector. The proposed B detector employs a cyclotron-style dipole magnet and emphasizes charged-particle tracking, vertexing, particle identification, mass resolution, and a flexible trigger system. There is no hadron calorimetry or muon system. The detector design envisions upgrades for higher luminosities and is compatible with a p-p collider at Fermilab. We anticipate first data collection in 1994. This detector is very similar to the central part of the SSC B spectrometer presented at Snowmass '88.

Contents

1 Introduction 1

2 Brief Summary of Bottom Physics Goals 2

3 Comparison to Other Approaches 4
- 3.1 e^+e^- machines . . . 4
- 3.2 Fixed Target Experiments at Hadron Machines . . . 5
- 3.3 Other Hadron Colliders . . . 5

4 Detector Overview 6

5 Detector 9
- 5.1 Dipole Magnet . . . 9
  - 5.1.1 Design of a New Dipole Magnet . . . 11
- 5.2 Silicon Vertex Detector . . . 12
  - 5.2.1 Introduction . . . 12
  - 5.2.2 Detector Geometry . . . 13
  - 5.2.3 Simulation of Vertex Detector Performance . . . 15
  - 5.2.4 Silicon–Straw Tube Matching Studies . . . 18
- 5.3 Silicon Vertex Detector: Devices . . . 22
  - 5.3.1 Double Sided Microstrip Detector . . . 22
  - 5.3.2 Silicon Pixel Detectors . . . 23
- 5.4 Tracking . . . 23
- 5.5 RICH Counters . . . 28
- 5.6 Time-of-Flight Counters . . . 29
- 5.7 Transition-Radiation Detectors (TRD's) . . . 30
- 5.8 Electromagnetic Calorimeter . . . 31

6 Front-End Electronics 32
- 6.1 Introduction . . . 32
- 6.2 Silicon Strip Front End Electronics . . . 32
  - 6.2.1 General Considerations . . . 32
  - 6.2.2 New Devices . . . 33
- 6.3 Straw Tubes . . . 34
- 6.4 RICH Counter . . . 34
- 6.5 TRD . . . 36
- 6.6 EM Calorimeter . . . 36
- 6.7 Development Costs . . . 36
- 6.8 Chips to be developed . . . 37

7 Trigger and Data Acquisition **38**
7.1 Introduction 38
7.2 Triggers 38
7.2.1 Topology Trigger 38
7.2.2 Electron Trigger 41
7.3 Data Acquisition 44
7.3.1 Basic Architecture of the Data-Acquisition System 44
7.3.2 The Event-Building Process 45
7.3.3 Processors 48
7.3.4 Fiber-Optic Digital-Data Transmission 48

8 Machine Issues for Tevatron **49**
8.1 Detector and Collision Hall Issues 49
8.2 Beam Energy 49
8.3 Luminosity 49
8.4 Length of the Interaction Region 50
8.5 Beam Size 51
8.6 Beam Pipe 51
8.7 Beam Halo 51
8.8 Compensation for the Dipole Field 51
8.9 The Detector Hall and Support Facilities 52
8.10 Summary and Status of Accelerator Issues 52

9 Prototyping and Test-Beam Efforts **53**

10 Cost **54**

11 References **56**

List of Figures

1 Detector Overview 6
2 Magnet Design 9
3 Magnetic Field Map 10
4 Magnetic Field Path Integral 11
5 Angle of Incidence 13
6 Silicon Vertex Detector 14
7 Pseudorapidity vs Hits per Track 15
8 Separation vs. Delta Separation 16
9 Pseudorapidity Acceptance 17
10 Track Multiplicity in Silicon 18
11 Silicon Strips Fired per Track 19
12 Path Length in Silicon 20
13 Residuals of Silicon-Straw Tube Matching 21
14 Double-Sided Silicon Readout 22
15 Straw-Tube Superlayer 24
16 Straw Tubes—median plane 26
17 Straw Tubes 27
18 Time-of-Flight Counters 30
19 Block Diagram of SSC chip set 35
20 Topology Trigger(I) 39
21 Topology Trigger(II) 40
22 Rate of Electrons 42
23 Data-Acquisition System Block Diagram 46
24 Receiver/Formatter Block Diagram 47
25 Collision Hall 50

List of Tables

1 CP Rates 3
2 Vertex-Detector Acceptance 17
3 Momenta Covered in the RICH Counter 29

1 Introduction

The Tevatron p-$\bar{p}$ collider, already performing beyond expectations, could produce up to 10^{11} $B\bar{B}$ pairs per year by 1994, thus making it a unique B facility. We propose to construct a powerful detector to study this sample of $B\bar{B}$ pairs, with the opportunity to make major contributions to our understanding of the standard model and beyond. It will likely take 10-15 years to explore this rich area of physics, as in the case of the K system. The proposed program will measure a spectrum of physics quantities leading towards a thorough study of CP violation in the B system and the best possible determination of the elements of the K-M matrix. A natural evolution is to continue this program at the SSC.

The task before us is sufficiently different from the goals of the existing or planned detectors that a new effort is needed. A great deal of effort has gone into the study of whether this experiment is feasible and competitive with other approaches. After more than two years of meetings, workshops, seminars, conferences and study groups, we feel very strongly that this experiment can be built and will play a major role in the particle physics program of the 1990's.[1,2,3,4,5,6] The experimental techniques and technologies required are essentially available. The next step is to begin a realistic engineering design which will capitalize on the existing technology but remain flexible to take advantage of advances in technology which are sure to come over the next several years. We are submitting the Letter at this time to elicit the support of the Laboratory in this endeavor and to be considered in the planning for the Tevatron Upgrade.

While the physics potential in the B system is great, the technical challenge to harvest it is formidable, and it will require considerable lead time to meet this challenge. We believe it is vital that a dedicated team of physicists begin full-time work now on a detector which could take data in 1994. The upgraded Tevatron provides the best opportunity for a combined program of major new physics measurements in the 1990's, and of detector development for B physics in the SSC era.

The prospects for eventual expansion of the B physics program are considerable. Factor-of-ten improvements are possible in (at least) two directions. The detector could be made to operate at a luminosity of 10^{32} rather than 10^{31} $\mathrm{cm}^{-2}\mathrm{sec}^{-1}$; and the experiment could be moved to the SSC where the B cross section is ten times larger.

This Letter outlines the physics of interest, the conceptual design of the detector, and its impact on the accelerator.

2 Brief Summary of Bottom Physics Goals

We propose a physics program to study the B system in complete and thorough detail. Many important measurements will be made on the way to the major goal for this program, CP violation in the B system. The richness of this program will likely require efforts beyond the initial experiment proposed here.

The experiment is designed to study B-decay modes useful for direct measurement of the elements of the K-M matrix. These measurements, if made with sufficient accuracy, will overconstrain the standard model and thereby probe possible physics beyond the standard model. For example, with precise measurements of the K-M matrix parameters one can learn about the Yukawa couplings of the Higgs sector.[10,11,12,13,14]

Here we list what can be studied with a sample of 10^{10} B's (and $\bar{B}$'s) from a p-$\bar{p}$ collider. This might be obtained in a run of 10^7 seconds at an average luminosity of 10^{31} cm^{-2}sec^{-1}, assuming $\sigma_{B\bar{B}} \sim 45$ μbarns.[7,8,9] The signal-to-noise ratio is ~ 1 $B\bar{B}$ pair/1000 inelastic events. We suppose the efficiency for reconstruction, including the invariant mass, of an all-charged decay of a B is 30%. The trigger efficiency is taken to be 20% if a particle/antiparticle tag is not required, and 3% if the tag is required. We would measure:

- the production cross section for B_d and B_s mesons, and B baryons.
- rapidity distributions for the above states.
- lifetimes for the above states.[16]
- branching ratios of $B \rightarrow$ all-charged modes that have a branching ratio $\tilde{>}$ 10^{-7}.[17]
- branching ratios of the charmless decay modes that have all-charged final states.[18]
- branching ratios of CP eigenstates, obtaining a sample of several hundred decays from modes with branching ratios of 10^{-5} or larger.
- gluon structure functions at low x from the longitudinal-momentum distribution of B production.[25]
- mixing in the B_d and B_s systems. The relative amount of mixing is predicted by the standard model.[19,20,21]
- the upper limit or rate for rare decays such as $B \rightarrow e^+e^-$ or $B \rightarrow Ke^+e^-$ as a signal for new physics.

- the strongest signals for CP violation in the B system, as discussed further below.

The experimentally accessible signal of CP violation in the B system is an asymmetry of the form

$$A = \frac{\Gamma(B \to f) - \Gamma(\bar{B} \to \bar{f})}{\Gamma(B \to f) + \Gamma(\bar{B} \to \bar{f})}.$$

Such asymmetries are expected to be in the range 0.05–0.30 for some favorable modes.[14,15] If the final state f is a CP eigenstate the relation between the measured asymmetry and the K-M matrix involves no knowledge of strong interactions (unlike all measures of CP violation in the K system, see [10] and references therein). But in this case, $f = \bar{f}$, so the identification of the parent B as a particle or an antiparticle must come from a tag based on the reconstruction of the other B in the event.

As examples we consider three modes, $f = K^+\pi^-$, $\pi^+\pi^-$, and ψK_S, of which the $K^+\pi^-$ decay is 'self-tagging,' while the other two are CP eigenstates and require a tag on the second B. The table lists the size of the CP asymmetry needed to produce a 3-σ effect in the proposed experiment, for the branching ratios and efficiencies also stated. The assumed branching ratio, Γ, for the ψK_S decay includes factors of 0.07 for $\psi \to e^+e^-$ and 0.3 for detection of the decay $K_S \to \pi^+\pi^-$. Of the 10^{10} B's produced only about 4×10^9 are B^0 or $\bar{B}^0$.

f	Γ	ϵ	$N_{\rm recon}$	A for 3 σ
$K^+\pi^-$	10^{-5}	0.06	2400	0.06
$\pi^+\pi^-$	5×10^{-5}	0.01	2000	0.07
ψK_S	10^{-5}	0.01	400	0.15

Table 1: The CP violation asymmetry needed for a 3-σ signal in various B-decay modes. ϵ is the assumed reconstruction $\times$ trigger efficiency. The number of reconstructed events is for a run of 10^7 sec at an average luminosity of 10^{31} cm^{-2}sec^{-1}, in which 4×10^9 B^0 and $\bar{B}^0$ mesons would be produced.

The information to be gained from B decays to CP eigenstates is conveniently characterized on a triangle, as advocated by Bjorken. An overconstrained determination of the K-M matrix consists of measuring the interior angles of this triangle. Each angle can be directly inferred from an asymmetry measurement. Thus a thorough study involves determination of the asymmetries in several decay modes in each of three classes of decays, all to CP eigenstates. A general-purpose B detector is certainly required for such a study.

3 Comparison to Other Approaches

3.1 e^+e^- machines

The main advantage of the Tevatron Collider and the SSC over existing and proposed e^+e^- machines is the larger B cross section at a hadron collider. The Lorentz boost of $B\bar{B}$ pairs produced at hadron colliders is also an important advantage over conventional $\Upsilon(4s)$ machines, as this permits reconstruction of the secondary decay vertex. However, e^+e^- machines have the advantage of much better signal-to-noise. The issue for the hadron machines is the experimental effficiency. The issue for e^+e^- machines is accelerator technology.

The key experimental technique which should permit extraction of the weaker B signal at a hadron collider is the reconstruction of the secondary decay vertex in a silicon vertex detector. In the case of charm physics, once this technique matured, experiments at hadron machines matched and now surpass those at e^+e^- machines.

The $B\bar{B}$ cross section at the $\Upsilon(4s)$ is about 1 nb, $\sim 45,000$ times less than at the Tevatron. On the Z, the $B\bar{B}$ cross section is about 5 nb. At a luminosity of 10^{32} $\mathrm{cm}^{-2}\mathrm{sec}^{-1}$, it is unlikely that present-day e^+e^- machines will observe CP violation.

Even assuming a 100% reconstruction efficiency for B's at an e^+e^- machine compared with 1% at a hadron collider, it would require a luminosity 500 times greater at the e^+e^- collider than at the Tevatron collider to produce an equal sample of reconstructed B's. Compared to the SSC, a luminosity 5000 times greater is required at the e^+e^- machines.

The prospects of studying CP violation have stimulated many proposals for high-luminosity e^+e^- machines. Amaldi and Coignet,[40] and Cline[41] have suggested symmetric linear colliders with luminosities of 10^{34} $\mathrm{cm}^{-2}\mathrm{sec}^{-1}$. Other ambitious approaches have been put forward by PSI, KEK, and SLAC.[42,43,44] More recently, SLAC and DESY have been studying the option of asymmetric collisions, yielding a boosted $\Upsilon(4s)$. With a luminosity of 10^{34} $\mathrm{cm}^{-2}\mathrm{sec}^{-1}$, the number of produced $B\bar{B}$ pairs per year will be on the order of 10^8. Even with 100% reconstruction efficiency, this sample would be only comparable to that obtainable in the first-generation experiment proposed here for the Tevatron. As yet, there is no realistic design for such a machine, which would probably be built only after the SSC.

LEP and SLC have powerful detectors, low-multiplicity events, and, since the B's come from Z decay, they are boosted which allows secondary vertex detection. If their luminosity approaches 10^{33} $\mathrm{cm}^{-2}\mathrm{sec}^{-1}$, they would be quite competitive with the BCD. However, it is unlikely they will produce enough events to address CP violation in the neutral B system. Even at 10^7 Z^0's produced per year this is less $B\bar{B}$'s than CESR produces now.

3.2 Fixed Target Experiments at Hadron Machines

The bottom cross section is $\sim$ 1000 times larger at the Tevatron collider than at fixed-target energies. Furthermore, the ratio of bottom to total cross section is about 3000 times larger at the collider. These advantages will permit a hadron-collider experiment to explore a much greater range of phenomena in the B system compared to a fixed-target experiment which must focus on very specific issues. Although fixed-target photoproduction yields a better $\sigma_{B\bar{B}}/\sigma_{\rm tot}$ than hadroproduction, the size of $\sigma_{B\bar{B}}$ is down by several orders of magnitude. Recent reviews on this subject have been given by Bjorken,[22] Garbincius,[24] and Sandweiss and Cox.[23]

3.3 Other Hadron Colliders

UA1 at the CERN $Sp\bar{p}S$ collider has already observed a large $B\bar{B}$ cross section. However the $B\bar{B}$ cross section is about a factor of 5 lower than at the Tevatron, and with the upgraded luminosity the Tevatron production of B's will exceed the CERN production by at least an order of magnitude.

A workshop held at BNL this summer explored the possibility of a bottom experiment in the proposed RHIC machine, running in a $p\bar{p}$ mode. Again the cross section is about a factor of 5 lower, but here the anticipated luminosity could be $> 10^{32}$ cm^{-2}sec^{-1}.

4 Detector Overview

The experiment is shown in figure 1. The design is driven by the need for large angular acceptance, good momentum resolution for low-momentum tracks, precision vertexing, and particle identification. Calorimetry is not important except for electron identification. The basic character of the detector is "central" with greater emphasis on the angular region $2° < \theta < 30°$ than in present detectors designed for W and Z physics. The main design considerations are listed here and greater detail is provided in subsequent sections.

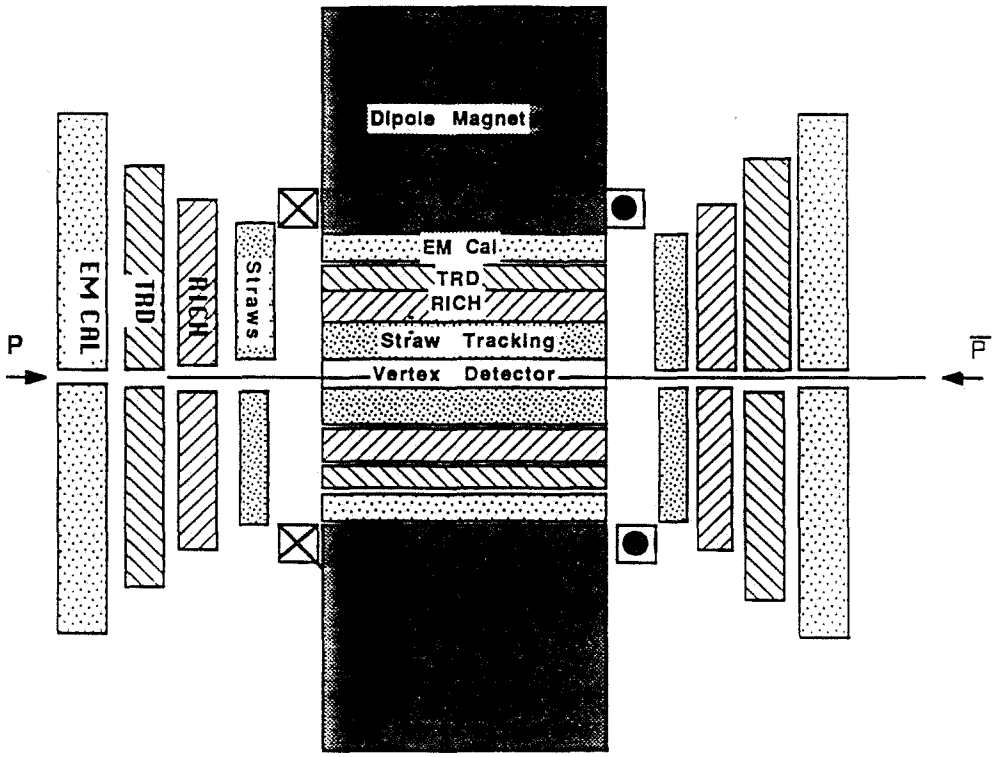

Figure 1: Overview of BCD detector.

- A dipole magnet is chosen to optimize the detection of tracks produced between $2° < \theta < 178°$ (pseudorapidity: $-4 > \eta > 4$). The kinematics of $B\bar{B}$ production are such that both forward and central tracks must be measured well in order to have a high geometric acceptance, while transverse momenta greater than 5 GeV/c are seldom of interest.[6] A dipole magnetic field oriented perpendicular to the beams is the best and simplest solution.

The magnet design calls for circular pole tips of 4-m diameter, separated by a 4-m gap.

- Even for small-angle high-momentum tracks, good momentum measurement can be obtained with a field of one Tesla in the dipole-magnet spectrometer. A low-field, large-diameter magnet is preferable for pattern recognition of low-momentum tracks.

- The gap size of 4 m permits a tracking system with 75-100 samples per track, the minimum acceptable number in a high-multiplicity event, while still accomodating the EM calorimeter, TRD, and RICH counters inside the coil.

- The vertex detector is designed to find the secondary vertices of the B particles with high efficiency, thereby reducing the combinatoric background. Also the ability to measure the time evolution of the states is particularly important for CP studies. Extensive Monte Carlo simulations[45] indicate that 3–D vertex reconstruction is necessary to achieve good pattern recognition, and that the system should have a worst-case impact-parameter resolution of < 20 μm. All tracks should intersect at least 3 planes with an angle of incidence $< 45°$. These requirements, along with the size of the intersection region, led to a hybrid design of barrels and planes using double-sided silicon. The detector is located outside the beam pipe, at 1.5-cm radius, to minimize effects of multiple scattering. Studies of this design, where tracking efficiencies were 100%, gave an efficiency for finding B vertices of $\sim 45\%$. A preliminary mechanical model of this detector design has been constructed.

- The vertex detector relies on the gas tracking system for most of the pattern recognition. The tracking system is designed for efficient and rapid 3–D pattern recognition of tracks over the full angular range. There are 75-100 hits along each track. The technology used is thin straw tubes arranged in superlayers. Straw tubes provide a measurement error of 40 μm per hit. Such high precision will allow a mass resolution of 20 MeV/c^2 and an extrapolation error into the silicon vertex detector of 50 μm. Good mass resolution is desirable to separate B_d and B_s, and to set a narrow mass window around the B as a rejection against combinatoric background.

- Particle identification is important in reducing the combinatoric background, especially for modes such as $B \to K\pi$ and $B \to p\bar{p}$. Electron identification is required for triggering and tagging the particle-antiparticle nature of the B. The design incorporates TRD's, RICH counters and an electromagnetic calorimeter over the full detector acceptance and for the full momentum range of the B decay products.

- The trigger and data acquisition system is designed to handle a luminosity of 10^{32} $cm^{-2}sec^{-1}$ and data-flow rates of GigaBytes per second. The trigger philosophy is to assemble the full event as soon as possible and pass it to a numeric processor where a variety of trigger algorithms can be implemented. The system is based on the latest communications-industry technology, which represents a new approach for high-energy-physics experiments and is suitable for SSC data rates.

5 Detector

5.1 Dipole Magnet

The dipole magnet for the BCD should have circular poles tips of 4-m diameter, a 4-m high gap, and a field strength of one Tesla. The large gap accomodates tracking and particle identification systems inside the magnetic field, while the circular pole tips maintain a field symmetry that simplifies the tracking algorithms. The magnet design and steel arrangement is shown in figure 2.

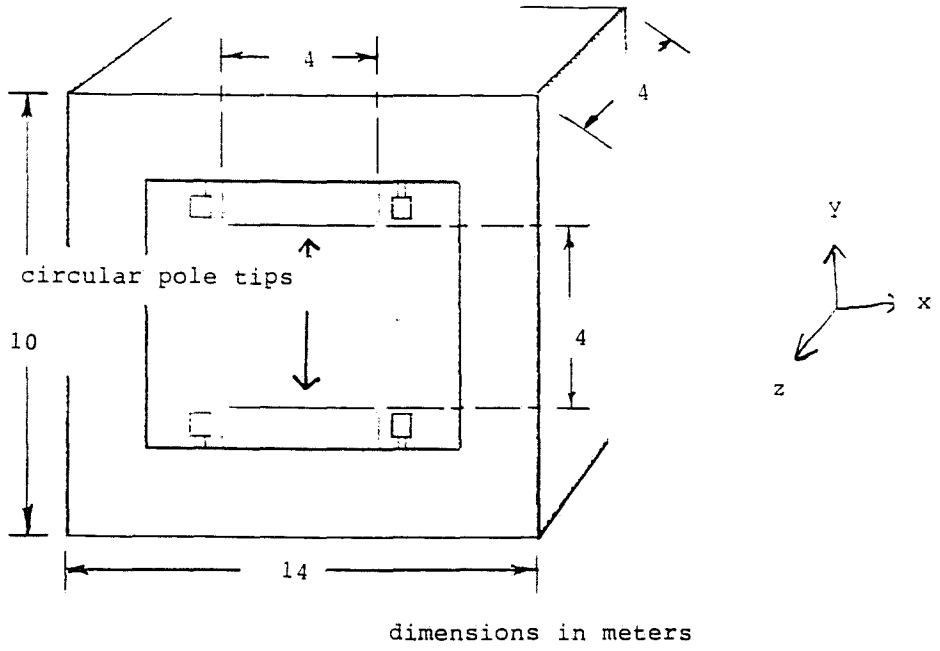

Figure 2: Dipole-magnet design and steel arrangement.

A comparison has been made with existing magnets that might be available on a time scale adequate for the Bottom Collider Detector. These are the CCM (Chicago Cyclotron Magnet), the MFTF (Magnet Fusion Test Facility) magnet, the Fifteen Foot Bubble Chamber Magnet, and the Berkeley 184″ Cyclotron magnet.

The CCM would be an ideal magnet for the B Collider, if its gap were opened from the present 1 m to the needed 4 m. It will utilized in the muon-physics program for several years. If it should become available, the cost of moving it to a new facility would be around \$750k.

The MFTF magnet has been turned on only once so this is a virtually new magnet. Only the superconducting coils of the MFTF magnet would be of use at

the Bottom Collider Detector. The BCD project would have to pay the cost of building the magnet yoke. Four of the existing ten coils could be used to achieve a 1-Tesla field. The cost of transport and installation are roughly estimated as $500k.

The Fifteen Foot Bubble Chamber Magnet has not been considered seriously for this project because it is being sought for an experiment at Gran Sasso. As for the MFTF magnet, a steel yoke would have to be built to incorporate the existing coils.

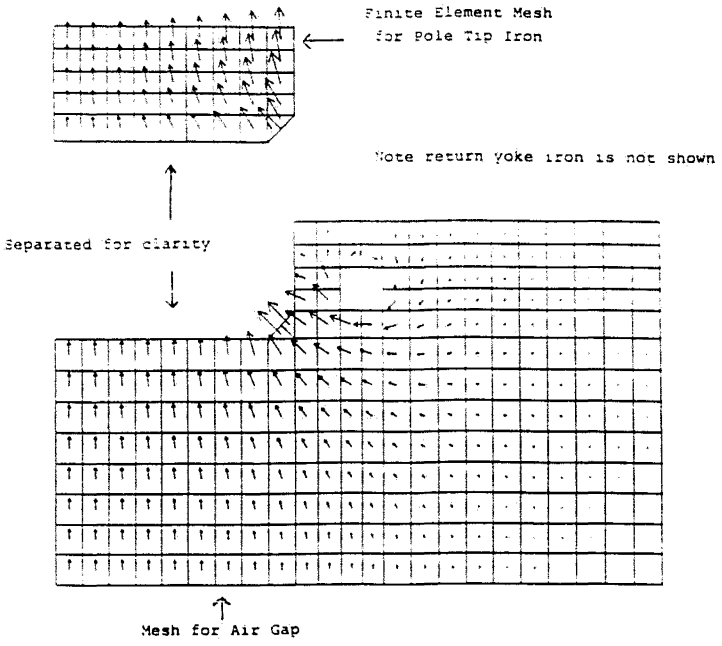

Figure 3: The vectors in each mesh element show the magnitude and direction of the magnetic-field flux density, for one quadrant of the magnet. At the center the value is about 1.14 Tesla, and near the corner of the pole it is about 3 Tesla (use of a B-H table in the ANSYS simulation would reduce this). The plots for the air region and the pole have been separated for clarity.

An attempt had been made to acquire the Berkeley 184″ Cyclotron Magnet for the Bottom Collider Detector. This was not possible because the magnet plates are only two inches thick (too many plates, too much rigging cost), they are mildly radioactive, and they are welded together into a yoke that also supports the crane at the Berkeley Cyclotron Building. The estimated cost of the procurement of this steel exceeds $1M, and was considered excessive. The copper magnet coils from the cyclotron are not considered useful because they are oil cooled and radioactive.

5.1.1 Design of a New Dipole Magnet

We are presently pursuing the design of a new dipole magnet. A study using the ANSYS finite-element analysis program is underway to explore several design issues.

As detailed in the Detector Overview section, the magnet-gap size is driven by the need for good momentum resolution and electron identification. This requires a long lever arm for tracking, and placement of the detector elements inside of the magnet. At present, the magnet modeling uses an overall dimension of $14 \times 10 \times 4$ meters for the yoke. The pole tips are 2 meters in radius. The weight of the magnet is estimated to be 3000 tons. With a 1-Tesla central field, the stored magnetic energy is 100 MJoule. A cost estimate is included in section 10.

Shown in figure 3 is the field map for this design. The $\int B\,dl$ from the magnet center outwards is typically 3 Tesla-meters, as seen in figure 4. With this, a momentum resolution of 1% or better can be achieved for all tracks with P_T less than 4 GeV/c.

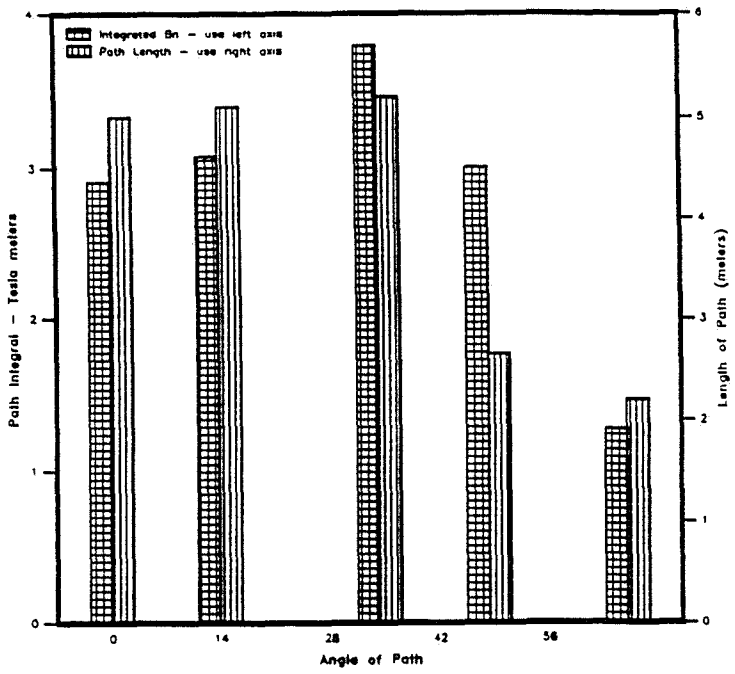

Figure 4: Shown here is the integral of the component of the magnetic field perpendicular to lines emanating from the magnet center at various angles with respect to the horizontal symmetry plane. The path length available is also shown.

An important physics issue relates to the transverse length of the iron yoke. The azimuthal symmetry of the field is destroyed by the presence of the vertical

return iron. By locating the iron further from the coils the field symmetry can be maintained. This results in a simpler field map and simpler track finding, which will be critical for the fast-tracking trigger of the experiment. The ANSYS simulation indicates that the vertical iron yoke should be about 3 m back from the pole tips to insure good field symmetry, while a minimal configuration with only 1-m spacing would cause considerable field distortion. The extra 2 m of steel in the horizontal yoke pieces adds a relatively small increment to the cost of the magnet.

Another important issue is the size and weight of the largest piece of the magnet. The coils are the largest pieces, about 5 meters in diameter including insulation. The weight of the largest steel piece would be limited to about 30 tons. In addition, we intend to bolt the magnet steel together allowing easy dismantling (for possible relocation at the SSC).

5.2 Silicon Vertex Detector

5.2.1 Introduction

The vertex detector is essential in extracting the B signal in a high-multiplicity environment. The clear association of tracks with a secondary vertex suppresses the otherwise overwhelming combinatoric backgrounds.

The lifetime, $c\tau$, of bottom mesons is about 360 μm. Secondary vertices must be reconstructable when their separation from the primary vertex is of this scale. We propose a microvertex detector based on silicon-strip detectors. Alternative vertex detectors utilizing the silicon-drift technique are also under consideration. Multiple scattering of charged particles and conversion of photons in the silicon detectors is a non-negligible problem. As a consequence we plan to use 200-μm-thick silicon, with double-sided readout.

The difficulty for precision vertexing in a collider experiment is that the secondary tracks emerge into the full 4π laboratory solid angle At present, tracking with silicon-strip detectors has been implemented only in geometries with near-normal-incidence tracks. However, because the interaction region in a hadron collider is spatially extended, there is no plausible geometrical arrangement of silicon planes which does not have some tracks at 45° incidence.

Figure 5 presents the angle of incidence (degrees from normal) on the silicon vertex detector for decay products of bottom mesons.

We anticipate that development of silicon detector technology will permit its use for 45°-incident tracks. A normally incident track will traverse the 200-μm thickness of a silicon detector giving a signal of 200 μm $\times$ 80 electron-hole pairs/μm = 24000 electrons. We plan to use 50-μm strip width, so that a 45° track would cross 70 μm of silicon per strip. The signal is then 70 μm $\times$ 80 electron-hole pairs/μm = 5600 electrons. It appears likely that VLSI readout chips for the silicon-strip detectors

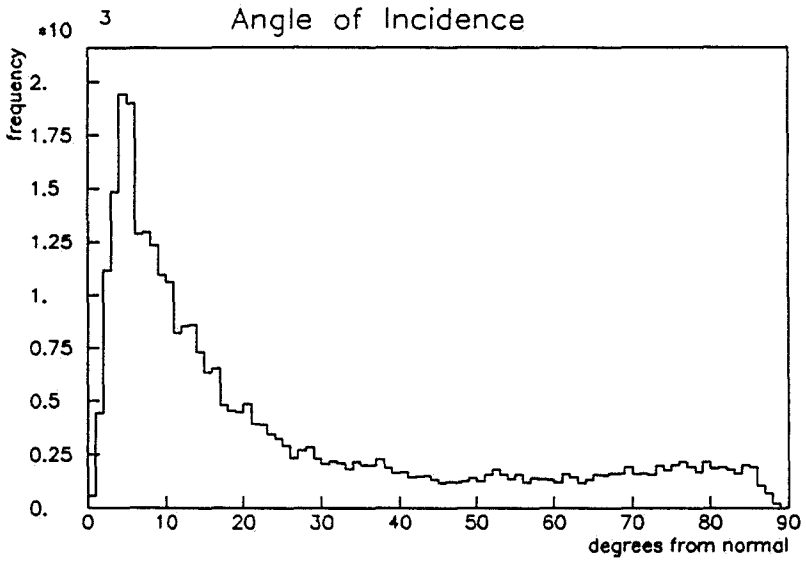

Figure 5: Angle of incidence upon the silicon vertex detector for bottom meson decay products (degrees from normal).

will achieve noise figures of 1000 electrons, which is entirely adequate. Indeed, if this noise level can be maintained even tracks with $\sim 0°$ incidence should be detectable, as these would yield about 4000 electrons.

5.2.2 Detector Geometry

The proposed detector geometry that has evolved over the past year is shown in figure 6.

The silicon vertex detector is logically segmented into two regions. The "central" region covers most of the interaction region with a combined geometry of equally-spaced silicon planes and three segmented barrels. The "rapidity-spaced" region covers the outer limits of the interaction region with silicon planes covering equal intervals in pseudorapidity. All silicon elements lie outside the beryllium beam pipe.

The beryllium beam pipe has radius 1.3 cm and thickness 400 μm. All (double-sided) silicon elements are of 200 μm thickness and have a strip pitch of 50 μm. Each disk has an inner radius of 1.5 cm and an outer radius of 13.5 cm. The detector consists of thirty-one parallel silicon disks and three segmented silicon barrels. The barrels have strips in z and ϕ directions, while the planes have strips in the x and y directions. The total length of the vertex detector is approximately 210 cm.

The central region of the vertex detector contains twenty-one planes with an

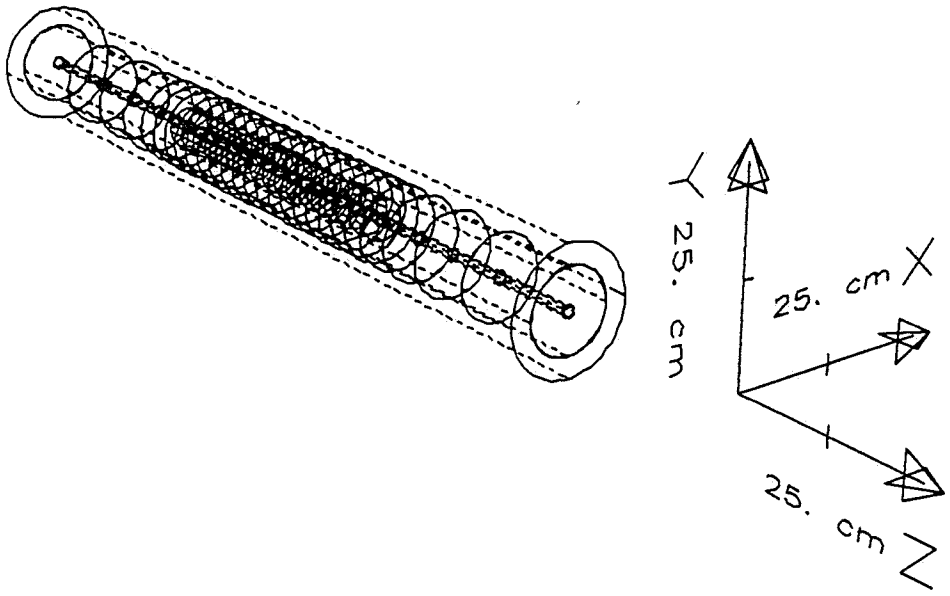

Figure 6: BCD Silicon Vertex Detector

interdisk spacing of 4 cm. The barrel segments are placed in the interdisk volumes and extend to the disk edges of the neighboring planes. The inner barrel radius is 1.5 cm; the middle silicon barrel radius is 5.0 cm; the outer silicon barrel radius is 10.0 cm. The central region extends from the center of the interaction region to $z = \pm 40$ cm.

The rapidity-spaced region is abutted to the central region and covers the outer limits of the interaction region. Silicon planes are placed every one-third unit of pseudorapidity, with the $\eta = 3$ planes equivalenced to the outer planes of the central region. Five rapidity-spaced planes extend from the ends of the central region.

This detector combines the features of the planar and barrel silicon geometries. Planes provide effective detector surfaces for particles traveling into the forward and backward regions, while barrels provide effective detector surfaces for radially-moving particles. The outer radius of the silicon planes has been chosen to be twice the interplane distance to guarantee three hits for all particles in the central region. Since the planes and barrels present relatively perpendicular surfaces to the particle tracks, this provides that all tracks that pass through the body of the detector will have three acceptable hits.

Figure 7 presents a scatterplot of hits per track versus B pseudorapidity for $B \rightarrow \pi^+\pi^-$. Hits are required to pass the cluster cut (see next section). (A shorter silicon vertex detector, designed for a shorter interaction region, was used in this study. Results for the long interaction region are expected to be similar.)

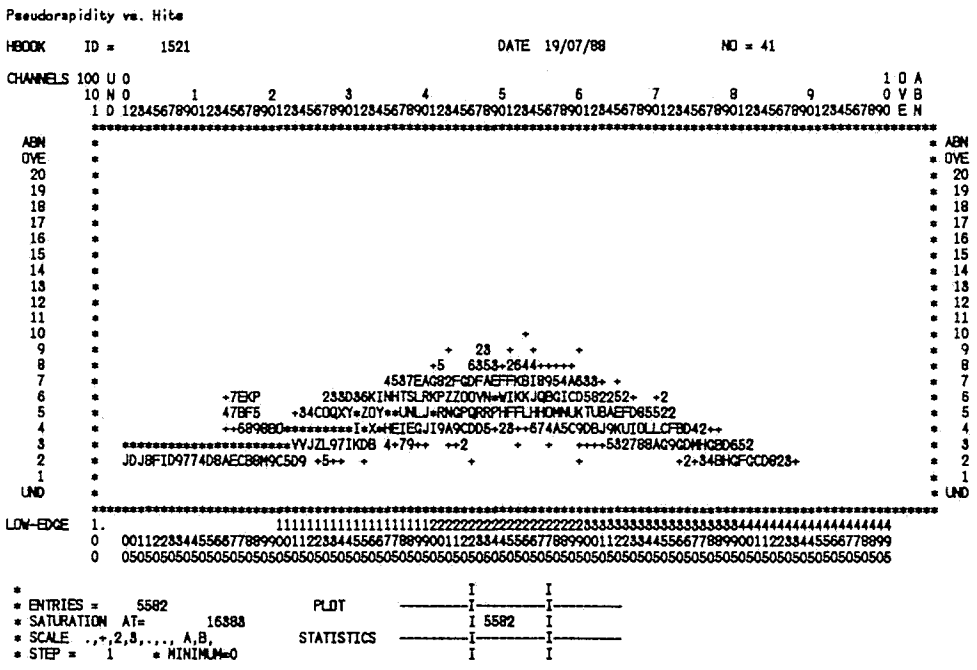

Figure 7: Pseudorapidity of the B meson versus the number of valid hits per track in $B \rightarrow \pi^+\pi^-$. Valid hits are those that pass the required cluster cut.

A model of the vertex detector has been built to address mechanical design issues.

5.2.3 Simulation of Vertex Detector Performance

PYTHIA 5.1 was used as the event generator for the simulation of the above design. Bottom meson events were generated for a p-$\bar{p}$ collider with 2 TeV center-of-mass energy. The minimum invariant mass of the hard-scattering parton subsystem was set at $10.5\,\mathrm{GeV/c^2}$; the minimum allowed transverse momentum was $0.0\,\mathrm{GeV/c}$. Decays of secondary particles were prohibited in the PYTHIA event generation—all particle decays were handled by GEANT3.

Bottom mesons only were selected from among the full PYTHIA-generated event for entry into GEANT3. Our objective was to determine whether reconstruction of bottom mesons would be possible using this vertex detector—one should first check that reconstruction is possible without any extraneous particles. Simulations were run using two decay modes: $B_d^\circ \rightarrow \pi^+\pi^-$ and $B_d^\circ \rightarrow \psi K_s^\circ$ ($\psi \rightarrow e^+e^-$). No magnetic field was present in the simulations, this being a preliminary design study.

Analysis was performed using GEANT3's knowledge of the particle decay. No

pattern recognition was used; the GEANT3 particle-decay chain was followed to identify descendents of each bottom meson. Both of the chosen decay modes allow a simple trigger—both provide two prompt, charged particles. Bottom meson events were accepted if both charged-particle tracks had at least two hits in the silicon detectors.

A cluster-size cut was imposed on the particle hits in the silicon detectors. The cluster size is defined to be the number of adjacent silicon strips which are fired by the passage of a single-particle track. Large cluster sizes present possible problems with signal size, hit location and pattern recognition. Hits with cluster sizes greater than four strips were rejected.

Particle tracks were defined by the first two (valid) hits on the track. Cuts on the vertex resolution were imposed on the quantity $S/\Delta S$, where S represents the distance of flight of the bottom meson and ΔS represents the three-dimensional distance between the reconstructed decay vertex and the true (Monte Carlo) decay vertex. $S/\Delta S > 5$ was the imposed cut. Figure 8 shows a scatterplot of S versus ΔS and the applied cut.

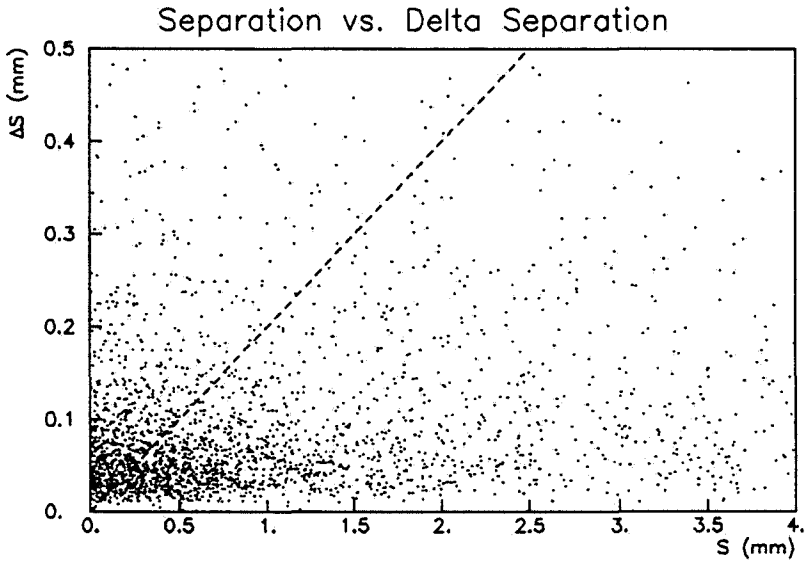

Figure 8: Scatterplot of separation S vs. delta separation ΔS for simulated $B \rightarrow \psi K_S$ events. The region below the dashed line contains events that satisfy the cut $S/\Delta S > 5$. Events with small S are predominantly produced in the central region, where the lower B momentum leads to a lower fraction of events surviving the cut.

Simulations were performed taking the the Tevatron interaction region to be a

Gaussian distribution of events with $\sigma = 35\,\text{cm}$. Vertex-detector acceptance as a function of the applied cuts can be seen in Table 2. Results are shown for both of the decay modes $B_d^\circ \to \pi^+\pi^-$ and $B_d^\circ \to \psi K_S^\circ$. Application of cuts is cumulative down through the rows of the table.

cuts	$B_d^\circ \to \pi^+\pi^-$	$B_d^\circ \to \psi K_S^\circ$
geometry cut	0.768	0.775
cluster cut	0.751	0.763
vertex cut	0.466	0.449

Table 2: Vertex-Detector Acceptance—interaction region with Gaussian distribution, $\sigma = 35\,\text{cm}$.

Figure 9 presents the accepted-pseudorapidity distributions for bottom mesons in the BCD silicon vertex detector. All cuts (geometry, cluster size, and vertex) have been imposed on this distribution. The distribution is for the decay mode $B_d^\circ \to \pi^+\pi^-$; the distribution for the decay mode $B_d^\circ \to \psi K_s^\circ$ is virtually identical.

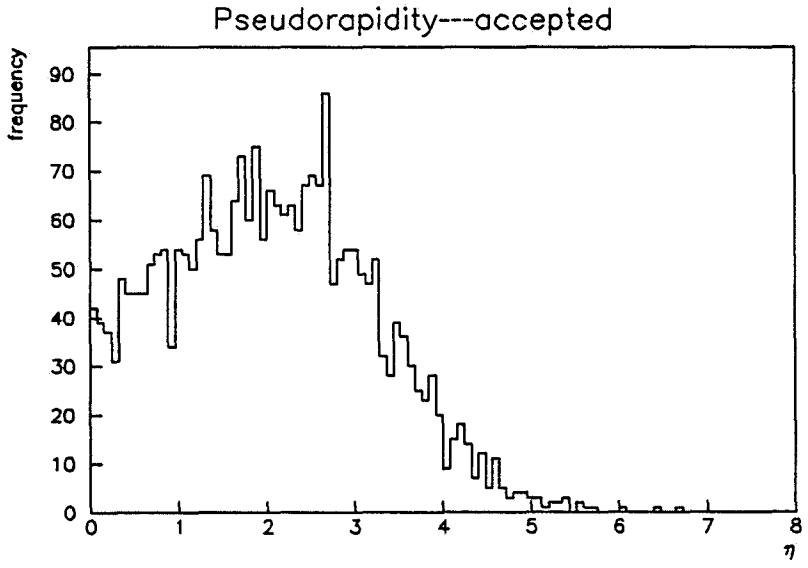

Figure 9: Pseudorapidity of accepted B mesons

5.2.4 Silicon–Straw Tube Matching Studies

General Character of Silicon Hit Distributions

Because a track has typically only three hits in silicon planes, the task of pattern recognition must be accomplished using information from the straw-tube chambers as well. Here we consider how well the silicon-hit information can be matched to a track as found in the straw-tube system. Difficulties arise when two or more tracks give closely spaced hits in the silicon planes all of which are potential matches to a track found in the straw-tube chambers. However, we find this confusion to occur in less than 2% of all tracks, using the simulation described below.

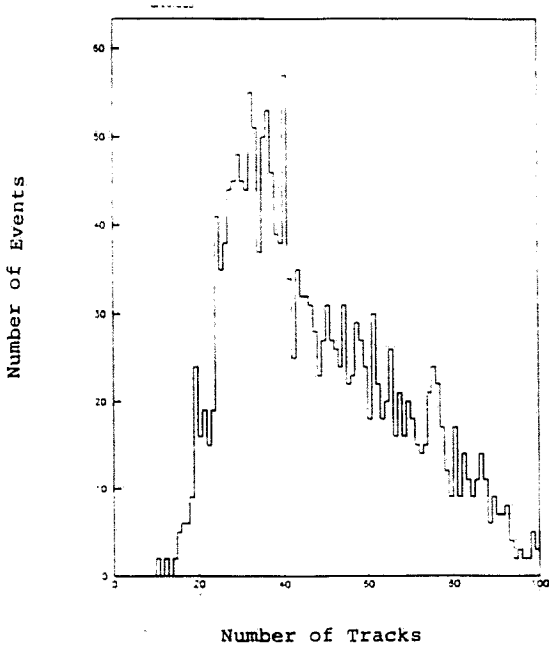

Figure 10: Multiplicity of tracks that strike the silicon vertex detector.

We studied simulated hit distributions in the silicon microstrip vertex detector by considering all the tracks generated in events containing the decay $B^0 \to \pi^+\pi^-$. The effects of decaying particles, photon conversions, multiple scattering in the detectors, *etc.*, are included. The charged-track multiplicity per event seen by the vertex detector is histogrammed in figure 10. The most probable number of tracks is 35 with a long tail on the high side. The number of strips fired per track, assuming a discriminator cut at 5% of minimum ionizing, is shown for the inner barrel detectors in figure 11a and for the planar detectors in figure 11b. The large number of strips fired per track in the barrel detectors is due to the cases where a small-angle track passes through many z-measuring strips. This condition is common since the distribution of track angles in space is highly peaked at small angles. This forward-

peaked distribution also results in relatively few multi-hit tracks seen in the planar detectors.

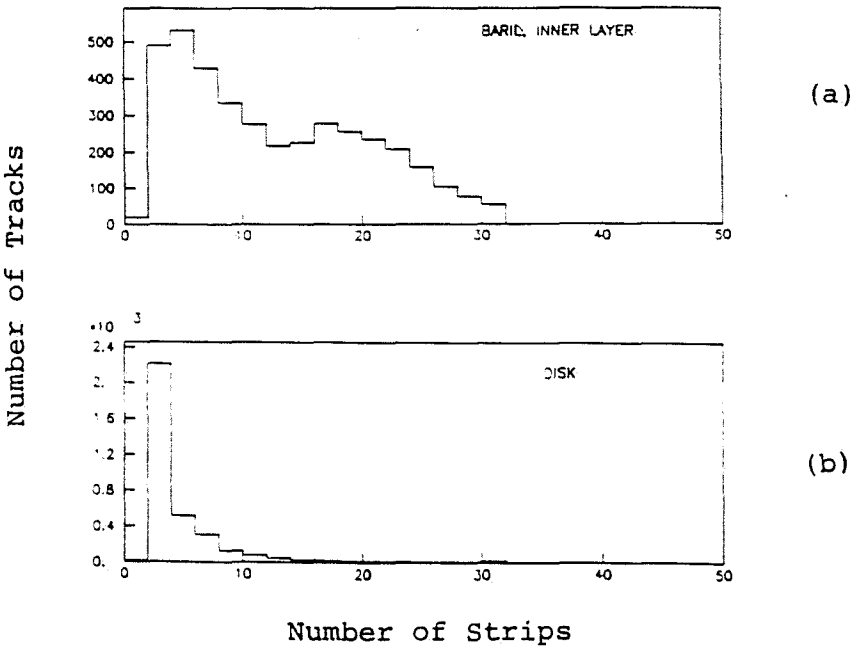

Figure 11: The number of silicon strips fired per track, with a discriminator cut at 5% of minimum ionizing. (a) Barrel silicon: (b) planar silicon.

The distribution of path length traversed through a single strip is shown in figure 12a for the inner barrel and figure 12b for the planes. The peaks at 200 μm are due to tracks at normal incidence to the detector, whereas the peaks at 50 μm are due tracks at grazing incidence and orthogonal to the strips. Hits due to path lengths much less than 200 μm could be suppressed by placing the discriminator cut above the 50-μm peak. This option will be explored in future studies. The very large path lengths are due to grazing-incidence tracks travelling along the length of a single strip. These very long path lengths are not disadvantageous to pattern recognition since they result in only one strip firing.

Effective Spatial Resolution of the Silicon Strips

The resolution of the silicon strips is affected by the number of silicon hits that can be associated with a given track found in the straw-tube system. If only one track passed through the window defined by the straw-tube track, then the silicon coordinate is given either by the single-strip coordinate or by the mean coordinate

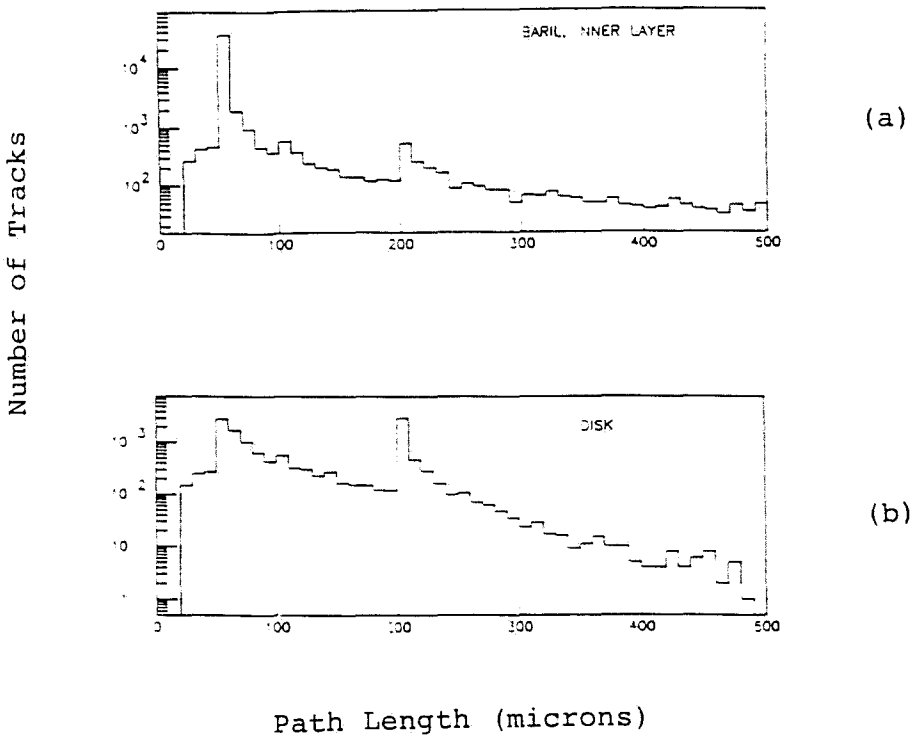

Figure 12: Distributions of path length in individual silicon strips. (a) Barrel silicon; (b) planar silicon.

if more than one strip has fired. The resolution in this case is illustrated by the histograms in figures 13a-c of the difference in position between the mean strip coordinate and the true (Monte Carlo) position of the track at the silicon detector. For the ϕ-measuring barrel strips and for the planar detectors the resolution is essentially due to the single-strip width of 50 μm. However for the z-measuring barrel strips, the residual distribution is widened due to tracks with multiple-hit patterns. Most of these tracks, however, will also be measured with better accuracy in the planar detectors.

If more than one track has passed through the window defined by the straw-tube track, then we do not know which silicon hit to assign to the track. One simple algorithm is to take the average of the hit coordinates within the window. The residuals in this case are shown in figures 13d-f for a search window of 150 μm, corresponding to a ± 1.5-σ cut for a 50-μm pointing resolution. The main effect is to enhance the non-Gaussian tails of the residual distribution. The fraction of search windows containing more than one track is 1.6% for the inner barrel and 1.4% for the planar disks. These fractions could be reduced if the strip lengths were decreased from the 5 cm assumed in this study.

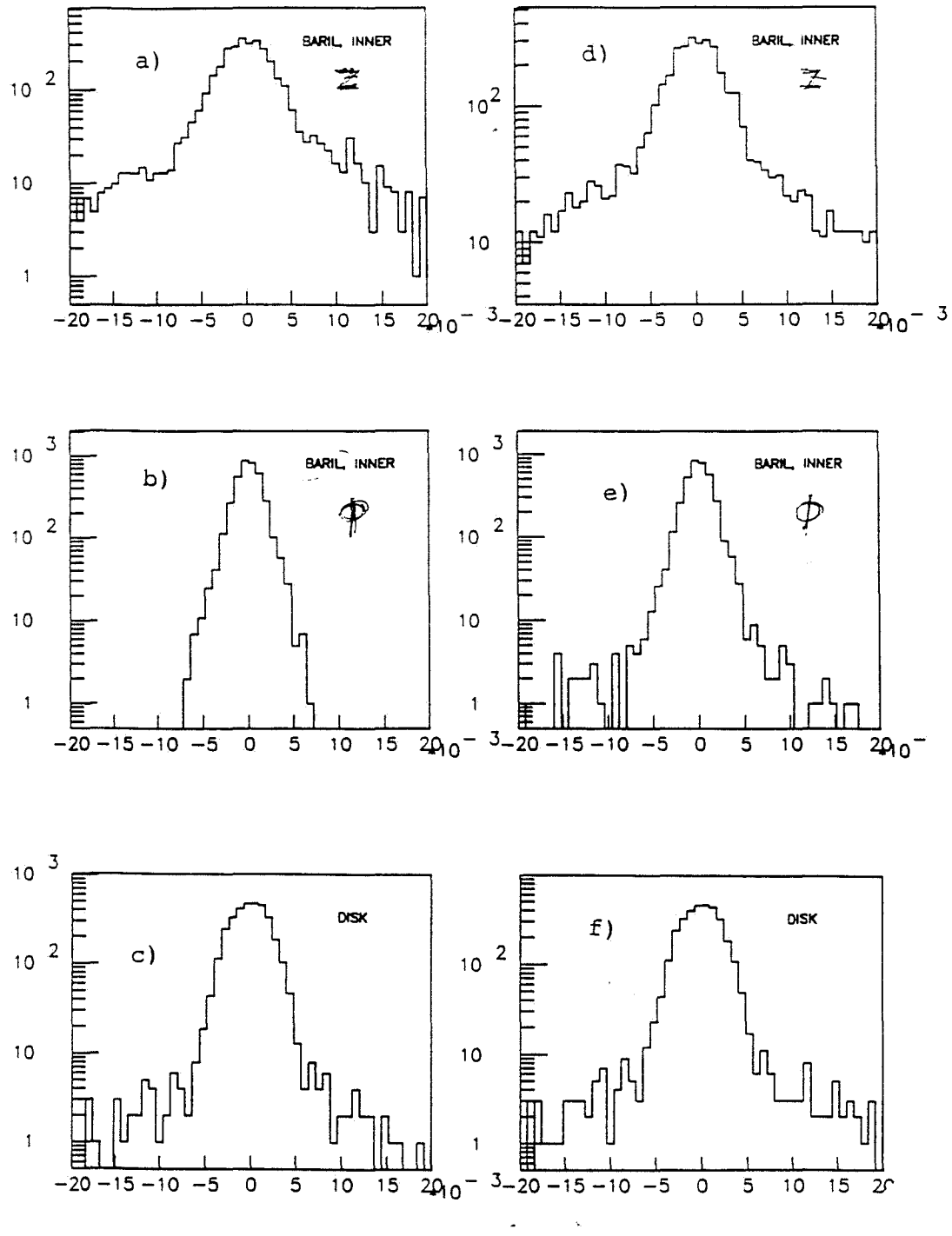

Figure 13: **(a-c)** Residuals between measured silicon hit positions and Monte Carlo generated positions; **(d-e)** Residuals based on the means of all hits in the silicon within a window defined by a track found in the straw-tube system.

5.3 Silicon Vertex Detector: Devices

Our present design uses the currently available double-sided silicon microstrip detectors. However, there is a world-wide effort to develop high-rate, high resolution pixel detectors. We plan to take advantage of these new devices as they become available. Below we discuss the microstrip detectors and two future possibilities.

5.3.1 Double Sided Microstrip Detector

We will use "double-sided" silicon microstrip detectors with the cathode strips oriented orthogonally to the anode strips, providing both an x and y measurement with a single silicon wafer. Such devices with dimensions 5 cm by 5 cm by 300 microns and 50-micron-pitch readout have been fabricated and tested.[46] An important feature is that capacitors integrated on the silicon couple the anode (high voltage) strips to the first-stage VLSI amplifiers. This type of detector will be used in the ALEPH and DELPHI experiments at LEP. A commercial manufacturer producing doubled-sided, capacitively-coupled detectors is Messerschmitt Buelkow Blohm (MBB) GmbH, Munich.

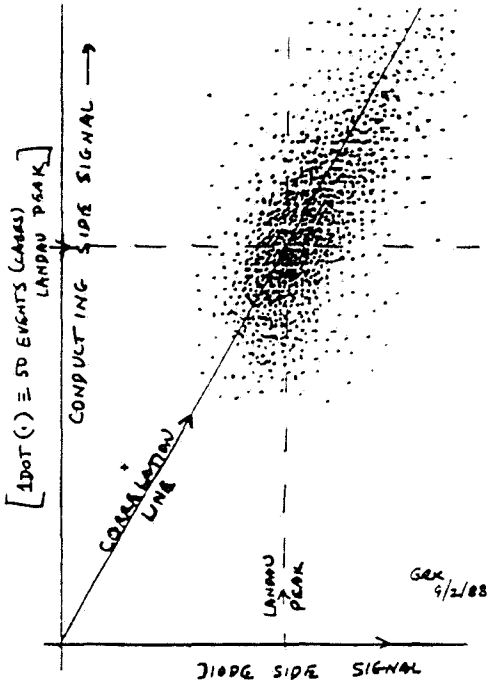

Figure 14: Observed correlation of pulse heights collected on opposite faces of a doubled-sided silicon strip detector.

Tests have been made on a double-sided wafer by the University of Oklahoma

group[60] to study the correlation of the pulse heights in the anode and cathode strips. If more than one track penetrates the silicon wafer, then it may be possible to pair the x and y hits since the pulse heights will be the same in x and y for a given track. The pulse heights for different tracks will vary according to the Landau distribution. Figure 14 shows the correlation of pulse heights observed on opposite sides of a silicon detector. This technique appears promising and makes the double-sided microstrip detector a quasi-pixel device.

5.3.2 Silicon Pixel Detectors

Silicon Detectors based on pixels rather than strips offer two potential advantages for a collider experiment. Each hit is recorded as an unambiguous space point, which clarifies pattern recognition and speeds use of the detector information in a trigger. Also, as the capacitance of a pixel is quite low, very small charges can be detected, and the active thickness of the silicon can be less than for a strip detector. When the detector thickness is comparable to or less than the pixel width the problem of angled tracks is largely removed.

We are investigating[61] the multianode silicon drift chamber of E. Gatti and P. Rehak, which implements 'virtual pixels' by recording the history of ionization electrons drifting towards a relatively small number of anode pads. Other promising techniques are those pursued by Parker *et al.*, by Shapiro *et al.*, and by Nygren *et al.*, who consider devices with true silicon pixels each with its own readout.

5.4 Tracking

Multiple scattering in and instrumentation costs of the silicon microstrip detectors (SMD's) do not allow a number of planes sufficient to reconstruct most tracks in three-dimensional space. The vertex detector must therefore be regarded as a precise vernier which improves the pointing accuracy of tracks reconstructed unambiguously in three dimensions by a larger tracking system consisting mainly of wire chambers.

This outer-tracking system must be able to reconstruct curved tracks coming from an arbitrary origin in a dipole magnetic field. This is a more difficult problem than that commonly encountered in collider detectors using a solenoidal field, in which the tracks in the azimuthal view are circles coming from a single, well-defined beam-intersection point. The tracking system must also measure momentum to an accuracy of $\pm 1\%$ in a 1.0-T dipole magnetic field, must deal with interaction rates of 5–10 MHz, and cannot have massive support structures such as end plates which would interfere with the nearly 4π electron trigger which will surround it.

Tracking designs based on straw tubes have several attractive advantages for this experiment. They require no massive mechanical supports, their small drift distance allows high rates, and the damage due to broken wires is very localized. However,

the support is distributed in the walls of the straws, which are a potentially large source of multiple scattering. The wall thicknesses must be reduced substantially below those now in common use if this design approach is to be viable.

DeSalvo[56] has proposed a design for an SSC central-tracking detector which is based on a large number of straws of 3.0-mm diameter and 30-μm wall thickness, pressurized to 3–4 atm. In addition to improving the resolution of the straws to 30–40 μm, pressurization adds to the rigidity and allows the reduction in diameter which leads to thinner walls. A "superlayer" of 8 rows of such tubes (figure 15) contains only 3.4×10^{-3} radiation lengths, resolves left-right ambiguities locally, and provides both a vector with 2-mrad pointing accuracy and an estimate of curvature. The multiple scattering in eight such superlayers induces a momentum resolution of 0.6% when distributed along 0.75 m in a 1.0-T field. The tracking design described here is based in large part on straws which are assumed to meet these specifications.

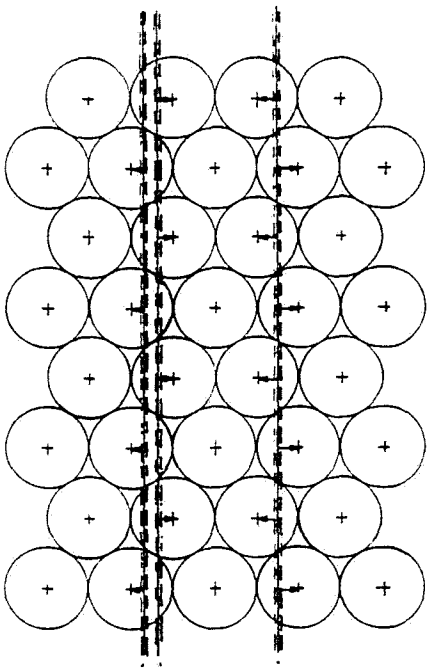

Figure 15: A "superlayer" of 8 rows of straw tubes.

The maximum radiation exposure which wire chambers can tolerate limits how close to the beam the straws can be placed, and leads in turn to a hybrid system with additional microstrip detectors for small-angle coverage. A conservative limit on the safe total multiplied charge in a wire chamber is[57] 0.1 Coul/cm per 10^7 sec at a gain of 10^5. The charged-particle flux into a normal area element Δa at a

perpendicular distance $r_\perp$ from the beam is well-approximated by[58]

$$(dN/da)\Delta a = (H/2\pi)(\sigma_{\text{inel}} \cdot L)/r_\perp^2 \qquad (1)$$

where $H = dN/d\eta$ near pseudorapidity $\eta = 0$, σ_{inel} is the inelastic cross section, and L is the luminosity. For the Tevatron, $H \approx 4.0$, $\sigma_{\text{inel}} = 40$ mbarns, giving $r_{\perp\text{min}} \approx$ 6-8 cm for 3-mm straws at $\mathcal{L} =$ 1-2 $\times 10^{32}$ cm^{-2}sec^{-1}. For an SSC detector it is estimated[58] that $H \approx 7.0$, $\sigma_{\text{inel}} = 100$ mbarns, resulting in $r_{\perp\text{min}}$ twice as large at the same luminosity.

A conceptual outer-tracking design using both straws and SMD's to cover pseudorapidities η out to 5.0 is shown in figures 16 and 17. It contains approximately 2×10^5 straws, plus an additional 10^5 SMD strips with 50-μm pitch located outside of the vertex detector.

Figure 16 shows the straw-tube panels and SMD's in a plan view section through the median plane of the central portion of one quadrant of the tracking system. Each straw-tube panel is a superlayer of eight rows of 3-mm thin-walled straws. In figure 16, the dipole magnetic field is perpendicular to the page and parallel to the wires in the x straw tube panels, which measure position in the bend plane. The u and v straw tubes are oriented at $\pm 14°$ to the x axis to provide information for the nonbend plane and to resolve the stereo ambiguity. Straw orientations with a large component of the magnetic field perpendicular to the wires are avoided because the effects of the Lorentz force are more difficult to deal with in reconstruction. Gas and voltage feeds and signal readouts of all straws are at the ends ± 80 cm above and below the plane of figure 16. The straw-tube x panels are arranged in an "egg-crate" pattern (with x panels both perpendicular to and parallel to the beams) to facilitate reconstruction of small-radius curved tracks.

Tracks in the forward and backward directions are reconstructed by u-x-v triplets of straw-tube superlayers and/or xy-uu' doublets of SMD's with double-sided readout, spaced approximately logarithmically along the beam direction z out to ± 320 cm from the interaction point. (Three straw-tube triplets and four SMD doublets are located beyond the largest z included in figure 16.) Because no straws are closer than 8 cm to the beam, tracks with pseudorapidity $\eta \leq 2$ are reconstructed by a combination of straws and SMD's; those with $\eta > 2$ are reconstructed almost entirely with the SMD's. In reconstructing tracks with this hybrid system it is therefore better to use straws and SMD's interchangeably in the same projection, which requires that the orientation of SMD strips be parallel to the straw-tube wires. In this design the x and u orientations of the straws and SMD's are identical. The SMD's have no v projection, but have instead additional large-angle stereo y and u' projections (perpendicular to x and u, respectively) to further resolve confusion among very small-angle tracks.

Figure 17 shows a section of the tracking system through the center of the detector and perpendicular to the beams. In this view the magnetic field and the x wires

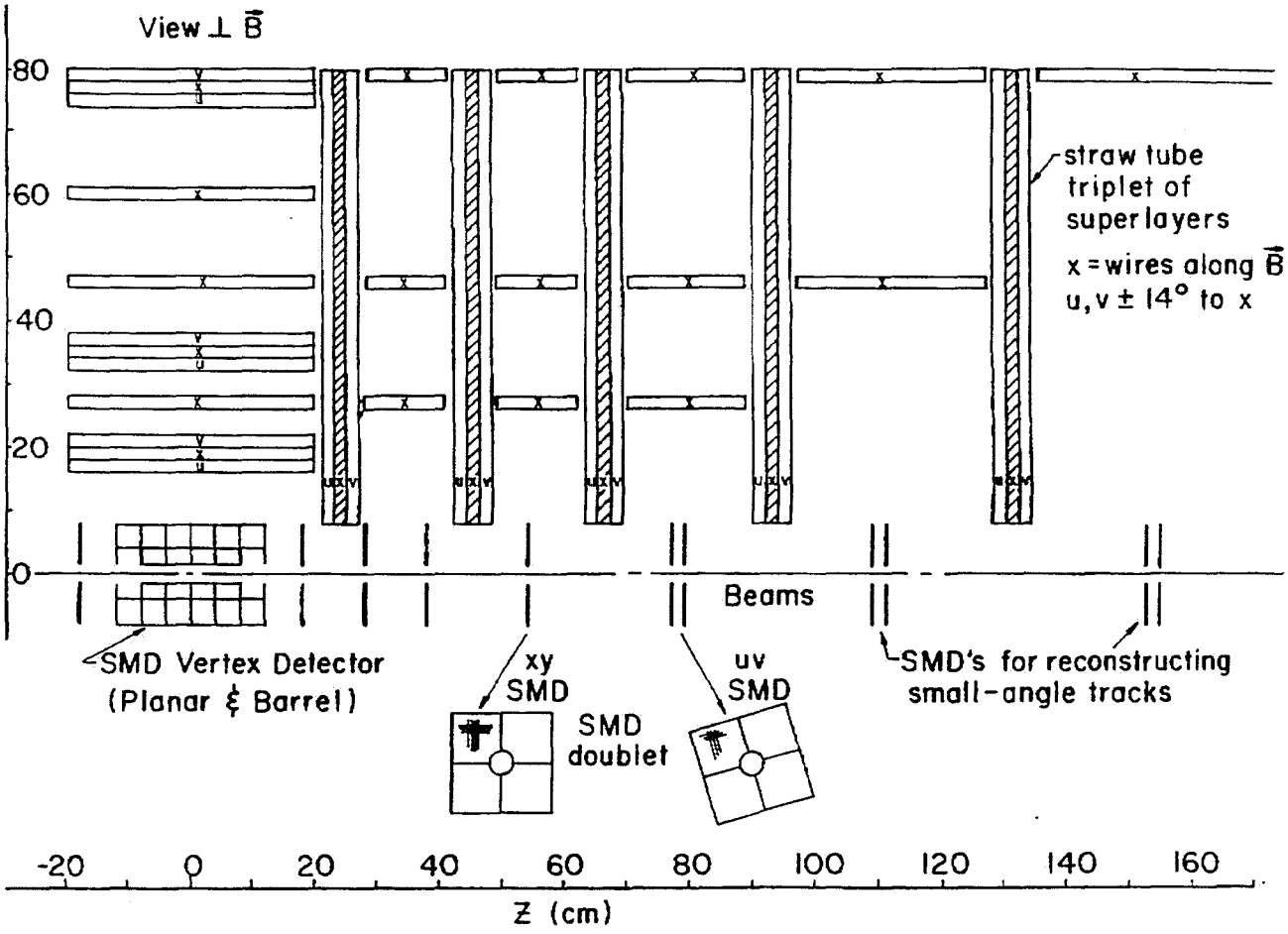

Figure 16: Plan view section through the median plane of one quadrant of the tracking system, showing the location of straw-tube panels and silicon microstrip detectors. The dipole magnetic field and the wires in the x straws are perpendicular to the page.

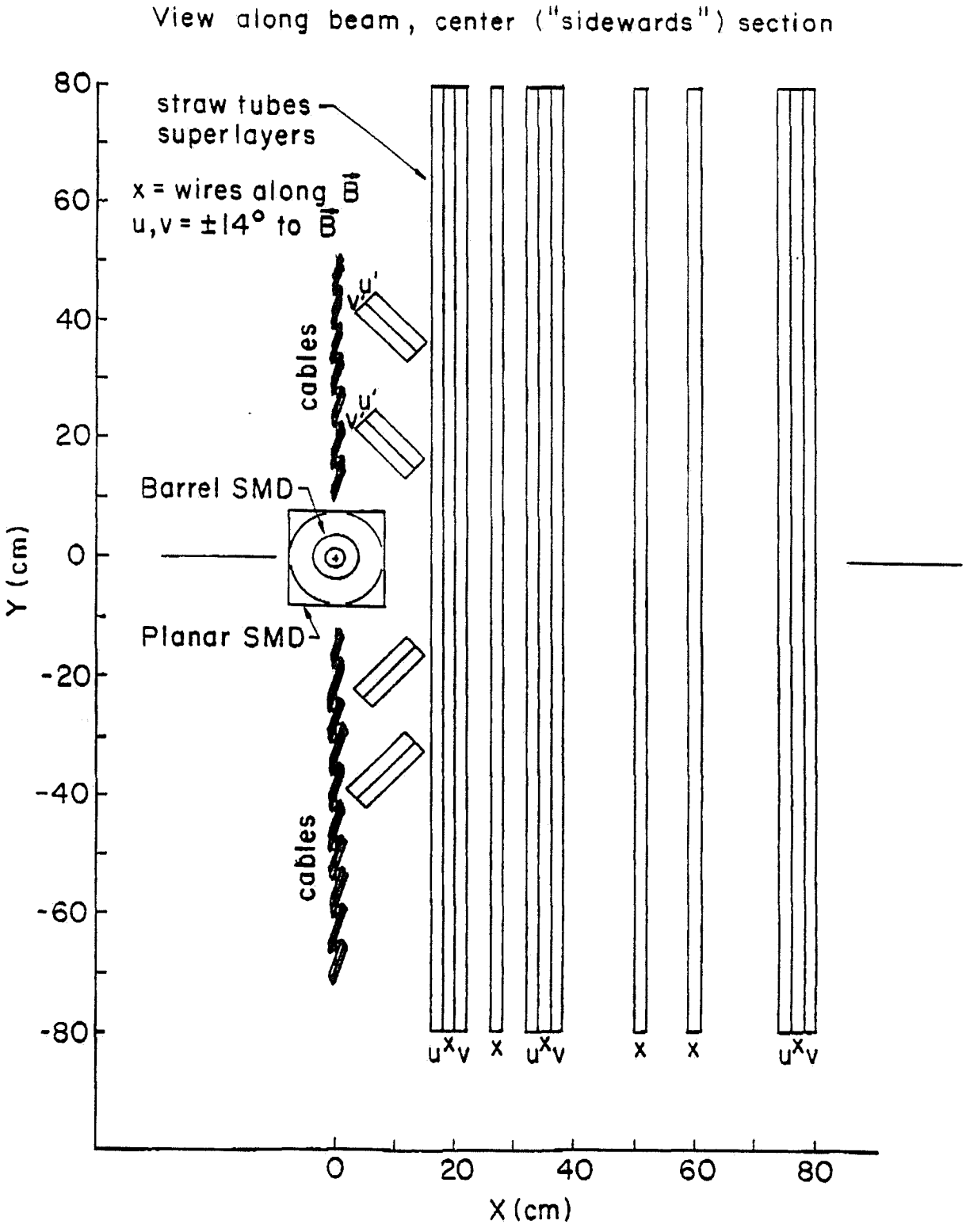

Figure 17: Section of the tracking system through the center of the detector and perpendicular to the beams. In this view the magnetic field and the wires in the x straws are vertical.

are vertical. Although the track density in this small-η region is low, it can be seen that the allowed large dip angles of $\approx 70°$ present difficulties, solved satisfactorily in this design, in obtaining a sufficient number of samples in each projection on tracks with large dip angle, and in extrapolating such tracks back to the vertex detector.

An estimate of the hit occupancy of straws and SMD strips can be made using equation (1). In the worst case of 3-mm straws 8 cm from the beam the occupancy is about 6%, while for a 50-μm SMD strip at 1.5 cm from the beam the occupancy is less than 1%.

The next step in designing the tracking system is to confront realistic simulated events in the detector with an actual trackfinding algorithm to determine whether the system has an adequate number of samples in each projection, and whether there is sufficient information to combine projections into three-dimensional tracks with high efficiency and small number of fakes. Work on such a trackfinding program is well underway. It is designed to deal with configurations of N superlayers of up to M samples each, provided only that all detectors in a projection are in the same rectangular coordinate system, and can find tracks of uniform curvature from an unspecified origin. On a longer timescale, a prototyping effort must be established to show that the very thin-walled straws on which this design is based can actually be built with the expected mechanical and electrical properties.

5.5 RICH Counters

The use of a ring-imaging Čerenkov counter (RICH) offers a means of π-K-p identification for transverse momenta up to about 4 GeV/c, as suitable for products from B decay. Low-momentum hadrons in the central region can be identified in a time-of-flight system described in a later subsection. In principle, a RICH counter can contribute to e-π separation, although this requires a somewhat different detector configuration than that proposed for hadron identification.

The detector is divided into two angular regions: forward, with $2° < \theta < 30°$; and central, with $\theta > 30°$. Then identification of of particles with transverse momenta up to 4 GeV/c implies the forward detector must operate with momenta up to 120 GeV/c, while the central detector must deal with momenta up to 8 GeV/c. The central region could be covered with a single RICH counter using a liquid radiator, such as C_6F_{14}, with a threshold of $\gamma_t = 2$. The forward region would require two counters: one with the same radiator as in the central detector to cover the lower momenta; and another with a gaseous radiator such as C_5F_{12} with threshold $\gamma_t = 17$. Table 3 summarizes the ranges of particle momenta and corresponding γ's over which the RICH counters should operate.

The space avalilable for the RICH counters permits a thickness of approximately 25 cm for the liquid counters, and 1 m for the gaseous counter. Complete coverage

	P (GeV/c) at $\gamma_t = 2$	γ at $P = 8$ GeV/c	P (GeV/c) at $\gamma_t = 17$	γ at $P = 120$ GeV/c
π	0.3	56	2.5	840
K	1	16	8.5	240
p	2	8	17	120

Table 3: Ranges of momenta and γ which should be covered by the RICH counters. $\gamma_t = 2$ for liquid C_6F_{14}, and $\gamma_t = 17$ for gaseous C_5F_{12}.

of the momentum ranges given in the table would require a position resolution of about 1 mm for detector of the Čerenkov photons. In turn this would require about 10^7 detector pixel elements. In the initial implementation we plan to use a wire-chamber detector with readout of cathode pads of size 8 mm × 8 mm, similar to that used in experiment E-665. For this about 10^6 elements are read out. The lower position resolution implies that π-K separation would be available only up to about 2.5-GeV/c transverse momentum.

The wire-chamber gas must be sensitive to UV photons for the detector to have reasonable efficiency. While most RICH counters to date use TMAE as the photo-sensitive vapor component, this must be heated to 70°C for optimal performance, and it is subject to radiation damage at relatively low doses. We prefer to use TEA, which functions at room temperature and is much less sensitive to radiation than TMAE. If TEA is used, then the windows between the radiator volume and the wire-chamber detector must be of CaF, which is somewhat more expensive than the quartz window suitable for TMAE. The quantum efficiency for TEA is lower than that for TMAE, in part because it is sensitive over a smaller range of wavelengths. However, because the optical dispersion of TEA is less than for TMAE the former has greater resolving power for the Čerenkov rings. The stated thicknesses of the radiators yield about 15 photoelectrons per Čerenkov ring with TEA.

An SSC R&D proposal[35] has been submitted by several members of the BCD collaboration to study the methods of triggering with fast RICH input. The results of this study will influence the option of electron identification via the RICH counters.

Preliminary cost estimates are based on the RICH counters of E-665 and SLD, and are summarized in section 10.

5.6 Time-of-Flight Counters

Particle identification in the central detector will be accomplished through the use of several devices. A time-of-flight system will be used to identify charged hadrons of momenta up to a few GeV/c, which complements the capability of the RICH

counters at higher momenta.

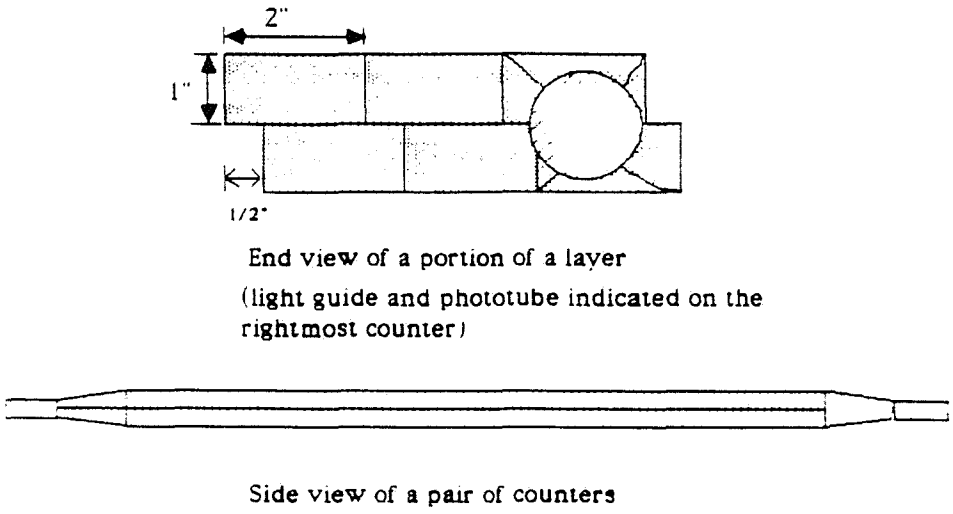

Figure 18: End and side views of the time-of-flight counters.

The system will be located 2 m from the beam, a distance constrained by the magnet-gap height. It will consist of two layers of $1'' \times 2''$ scintillator, staggered by $\frac{1}{2}''$, for a total of 640 scintillators. The scintillator will be chosen to have a fast rise time and long attenuation length. Adiabatic light guides will connect a set of two scintillators, ganged in depth (see figure 18) to two $2''$ photomultiplier tubes, one on each end. The phototubes must either operate in the magnetic field, or be located outside it.

The p.m. signals will be split, with part of the signal going to an ADC and part to a TDC. The ADC pulse height will be used to correct the TDC time, yielding a measurement which is better than that achievable using rise-time-compensated discriminators. The TDC's need to have a 50-ps least count. The stop time as measured by each tube will be combined to yield a single measurement for each track. Using this method, it should be possible to achieve a timing resolution of 70 ps per track. For counters at the 2-m distance, this allows a 1-σ separation of K's from protons at momenta up to 8 GeV/c, and π's from K's up to 4 GeV/c.

5.7 Transition-Radiation Detectors (TRD's)

Separation of e's from charged pions will be aided by multiple layers of thin-sampling TRD's.[38] The combination of tracking information with the transition-radiation

signal should permit an online pion-rejection factor of 50 in the TRD. The utility of the TRD's at small production angles needs further study.[39]

5.8 Electromagnetic Calorimeter

The calorimeter functions primarily to aid in electron identification, rather than providing a precision energy measurement. As such, position resolution is more critical. We thus have the option to use a sampling calorimeter (as opposed to total absorption in BGO or lead glass, *etc.*).

The calorimeter should have tower geometry, with three longitudinal samplings per tower. This feature should permit an online rejection factor of several hundred for charged π's. The transverse size of the towers should be sufficient that the energy measurement is of only a single particle with 99% probability, leading to a tower count of 10^4 given an average multiplicity of 100. A position-sensitive detector will be placed between the first and second layers of each tower to reject overlaps of a charged pion with a photon from π^0 decay. For this a two-track resolution of about 1 cm is desirable.

The particular form of the electromagnetic calorimeter is not specified at this time.

6 Front-End Electronics

6.1 Introduction

The front-end electronics will be in the form of custom integrated circuits, permitting low-cost and low-power readout of the large number of detector elements of the Bottom Collider Detector. All of the various chips proposed here are straightforward extrapolations or reconfigurations of presently available devices.

The front-end electronics should operate at a collider interaction rate of up to 5 MHz. Many of the readout signals are to be used in the first-level trigger, and all of the signals must be buffered during the 1-2 μs formation time of this trigger. VLSI chips (Bipolar and CMOS as appropriate) are mounted directly on the detector elements in order to amplify, shape, store and sparsify the signals. The basic module is a small number of high-channel-density ASIC's covering a relatively small physical area, tied together on a low-mass printed-circuit board. As this board serves many detector channels, the number of cables or optical fibers to the outside world is small.

Here we discuss the individual systems.

6.2 Silicon Strip Front End Electronics

6.2.1 General Considerations

The compact configuration of silicon planes will require local signal processing with a high degree of multiplexing. The signal processing speed must be compatible with the 2.5-MHz interaction rate at $\mathcal{L} = 5 \times 10^{31}$ cm^{-2}sec^{-1}. Analog and/or digital delay must be provided to allow time for a trigger decision to be made. Finally, the readout time must be minimized by use of sparsification. The first generation of suitable low-power "microplex" integrated-circuit readout electronics partially meets these goals and probably will be suitable for $\mathcal{L} < 10^{31}$ cm^{-2}sec^{-1}. The exact limitations will be established by testing. For $\mathcal{L} > 10^{31}$ cm^{-2}sec^{-1}, we will employ the chips currently under development for the SSC. The currently existing devices include the MPI CAMEX,[48,49] the LBL SVX[50] and the RAL MXI.[51] Below we comment briefly on the known properties of these CMOS chips.

MPI CAMEX

The 64- and 128-channel CAMEX chips were developed at the Max Planck Institute (Munich) for the ALEPH experiment at LEP. These chips are now being made commercially by ELMOS, Duisburg, Fed. Rep. Germany. The 64-channel chip has a power dissipation of about 120 mW and has been operated with a sampling time of 133 ns with a noise figure of 275 + 30 C_D[pF] electrons r.m.s., where C_D is the single-strip capacitance. The dependence of noise on readout speed has not been

measured. Radiation damage measurements have been made with a Co^{60} source and a broad-band x-ray source with a maximum energy of 200 KeV. The tolerance is not known for minimum ionizing particles and slow neutrons.

LBL SVX

The SVX chip was developed by Lawrence Berkeley Lab for the CDF detector at Fermilab. It has 128 channels with both analog and digital circuitry, and a total power dissipation of about 200 mW. The analog section provides up to two pairs of double-correlated samples, and in addition there is a comparator (discriminator) with a setable threshold. The readout has a fast-scan feature which selects only those channels with signal above threshold, and, if desired, the neighboring channels. In the fast-scan mode, channels not requiring readout take up no time in the readout cycle.

MXI

This chip was developed by Rutherford Appleton Lab for the DELPHI experiment at LEP and is a CMOS version of the Stanford Microplex[52] chip used in FNAL E-665[53] and Mark II at SLC. The RAL chip has 128 channels and dissipates 55 mW per chip. There are two storage capacitors per channel allowing a single pair of correlated samples. Radiation damage has been studied using a Co^{60} γ source.

6.2.2 New Devices

The current generation of VLSI silicon-strip readouts do not allow for a trigger delay. This problem is being addressed by the silicon strip readout system being developed by Seiden *et al.* at U. C. Santa Cruz. In their approach, an analog amplifier and comparator chip (AACC) provides a fast (15-ns rise time) signal that is digitized to 1 bit (yes or no). The bits are stored in a level-1 memory that is 64 cells deep and is clocked at the bunch-crossing rate of the accelerator. This is followed by a 16-cell-deep level-2 memory.

Another approach is to employ an analog pipeline for a trigger delay. Such a VLSI device with 10-MHz clock speed is being developed for the ZEUS calorimeter at HERA by a DESY-Fraunhoffer-Madrid-Nevis collaboration.

Other considerations are described briefly below.

- A possible feature for the front-end electronics is a pulse-height sum with a separate threshold used to reject greater-than-minimum-and nuclear interactions.

- It is important to note that driving the signal off the chip is very power consuming. The data readout would be over a few (10-100) optical fibers. Overall power-cost per channel probably can be kept to 1-3 mW/channel. With 10^5 channels, this is still considerable heat to dissipate.

- Bonding techniques such as indium bump bonding or tab bonding may make possible the connection of the CMOS chip to the detector strips at these high densities.
- We estimate about \$20/chip plus \$30 for packaging or about \$0.50/channel.

6.3 Straw Tubes

We take as our model the TVC chip set developed at U. Penn for the SSC (see figure 19). The bipolar amplifier/shaper/discriminator could be used directly and the CMOS TVC/analog store could be used but with a slower clock, typically 5-10 MHz.

The system would consist of the preamp/shaper/discriminator followed by the TVC/analog store/ADC/readout control chip. The bipolar chip will have four channels and the CMOS chip will have 8 channels. In addition the system would need a data-collection chip (digital CMOS) for every 8-32 TVC chips. Total power costs would be about 20 mW per channel. A possible arrangement would have a thin printed-circuit board mounted on the ends of 128 straws, with 32 bipolar chips, 16 CMOS TVC chips, and one data-collection chip, in addition to discharge protection and bypass and coupling capacitors for the straws. The cost would be about \$2-3 for the bipolar chip/channel, \$1-2 for CMOS, \$0.25 for the data chip and \$0.50 for mounting, for a total of $<$ \$6/channel.

It will be useful to include segment-finding electronics for some of the superlayers. This should be possible by adding a CMOS digital-logic chip in parallel to the CMOS TVC chip. Found segments would then be shipped to the trigger system. The increase in power cost should be only about 10% assuming a high level of multiplexing.

6.4 RICH Counter

A readout system identical to that for the silicon strip detector is planned for this system. The RICH counter will have pad sensors whose signals will be similar in magnitude and shape to the signals from silicon strips. While the electronics for this detector will be identical to the silicon system, the mounting problems and power-density problems are much different. Individual pads will have to feed in over a fairly large area to a single CMOS chip: small groups of these front-end chips would then feed into a local data-collection chip and thence out to the data-acquisition system. The relatively low density of connections will keep the per channel cost much less than in the silicon case ($<$ \$0.25/channel).

DRIFT CHAMBER ELECTRONICS

TIME MEASUREMENT

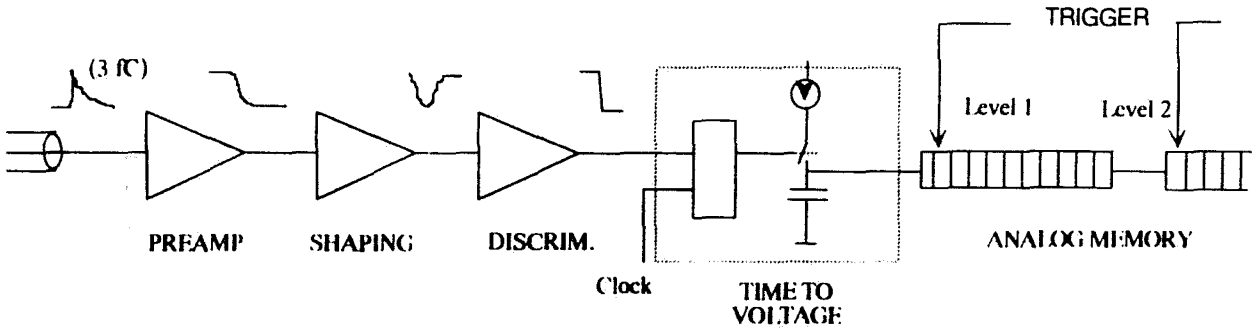

REQUIREMENTS:

TIME RESOLUTION:	< 0.5 ns
DOUBLE PULSE RESOLUTION:	20-30 ns
MEMORY STORAGE:	1 us
ENC:	700-1000 e-
POWER:	< 10-15 mW
RADIATION HARD:	1-10 Mrad
SIZE:	< 1 sq. cm/channel

Figure 19: Block Diagram of SSC chip set

6.5 TRD

The TRD detector will have many separate layers of wire-chamber detectors, The electronics must sense clusters on individual wires, but the linking and majority logic to find tracks would be done outside the detector. While the silicon-detector CMOS system would be appropriate in terms of signal handling, the relatively low density, linear arrangement of wires would probably argue for the development of a lower-channel-count CMOS device that could be more easily tied to the chamber. For the lower-channel-count device (*e.g.*, 8–16 channels), the effective power per channel would go up slightly because of the increased output-drive requirements. The cost in dollars however, would scale almost directly with TRD area and should be equivalent to the RICH-counter costs per channel.

6.6 EM Calorimeter

The calorimeter would use a readout system similar to that of the straw tubes in the sense that a bipolar front end would feed a CMOS delay-and-encode section. However, the calorimeter requires charge measurement over a large dynamic range and may or may not require an acurate time measurement. Thus the bipolar chip will necessarily require rather more power (for the dynamic range) and the CMOS chip will require more area for storage capacitors (high- and low-charge ranges). In addition the calorimeter will serve as one of the primary triggering detectors and must provide fast signals out of the detector to the central triggering system. These signals will require > 40 mW per output, but the trigger outputs will be sums of local channels so that the total power burden is not greatly increased. If a suitable clustering algorithm can be defined and tested, it is possible to imagine shipping only cluster position and size information to the trigger system, greatly reducing the burden on and increasing the power of the trigger. We estimate that the total power requirement per channel would be about 30 mW and the cost per channel would rise slightly to $< \$7$. Mounting and cooling is least restrictive in this region and we anticipate no major problems for the calorimeter system.

6.7 Development Costs

The purely digital CMOS chips are amenable to commercial design and production, but the analog bipolar and mixed analog/digital CMOS chips will require careful simulation and design. Each of the analog designs will require about three to four months of an expert engineer's time to develop and an additional foundry cost of order \$25K per chip (per run). Digital CMOS designs can be handled commercially for order \$40K per chip with only block-level schematics provided to the foundry.

6.8 Chips to be developed

1. CMOS preamp/discriminator/delay/encode - 128 channels.
2. CMOS data-collection fiber driver, all digital, possible to design and fabricate commercially.
3. Bipolar preamp/shaper/discriminator - 4 channels, after the design of Newcomer, *et al.* - should need little work.
4. CMOS TVC analog-store/encode - 8 channels, Penn/Leuven design - may need only to be appropriately packaged.
5. CMOS preamp/discriminator/delay/encode - 8 chan, a subset of design 1.
6. Bipolar high-dynamic-range preamp/shaper/discriminator - 4 channels, variation of 3.
7. CMOS TVC Charge analog-store/encode - 4 channels, variation of 4.
8. Clustering and trigger-driving chip, analog CMOS, perhaps based on neural-net work at Penn.

7 Trigger and Data Acquisition

7.1 Introduction

We propose a trigger architecture in which a first-level hardware trigger is followed by a software trigger implemented in an online array (farm) of numeric processors. The philospohy of this approach is that any trigger decision which uses digital information should be made in commercial, programmable processors.

The first-level trigger should reduce the rate by a factor of 50 in a 1-2 μsec decision time, so that even at a luminosity of 10^{32} cm^{-2}sec^{-1}, for which the interaction rate is 5 MHz, at most 100 kHz of events are presented to the numeric processors. The data from the various detector components can be organized into event records at a 100 kHz rate via the "barrel-switch" technology of the telephone industry. The numeric processors, perhaps 2000 in total, each are the equivalent of 30-50 VAX 780's. The archival event rate will be about 1 kHz, which can be accomodated by video-cassette tape drives.

Two types of first-level triggers will be implemented. A simple trigger is based on a requirement of 1 or 2 tracks above a mimimum-P_T cut of 2-3 GeV/c. More ambitious is a trigger on an electron above a mimimum-P_T cut of only 1-1.5 GeV/c, which would also provide a tag on the triggering B as particle or antiparticle.

Each of these first-level triggers is then completed in the numeric processors. The topology trigger is followed by a requirement of a reconstructed secondary vertex, while some aspects of the electron trigger can only be implemented with the power of the numeric processors.

7.2 Triggers

7.2.1 Topology Trigger

The B mass, as well as its typical production transverse momentum, are large compared to the average transverse momentum of particles from p-$\bar{p}$ collisions. Hence a "stiff-track" trigger will be enriched with B's.

Figures 20a and 21a show the number of tracks having transverse momenta above a given value in events containing a $B \to \pi^+\pi^-$ decay, and any B decay, respectively. For comparison, figure 20b shows the same distributions for all events (according to an ISAJET model) not containing a B, while figure 21b shows these distributions for all events.

We infer from figure 21b that with a requirement of 1 track above $P_T = 3$ GeV/c, a factor of 50 reduction in the trigger rate can be obtained. Then the efficiency for the $B \to \pi^+\pi^-$ decay is still 90%, as seen in figure 20a. Also, the efficiency for all B decays remains about 25%, as seen in figure 21a.

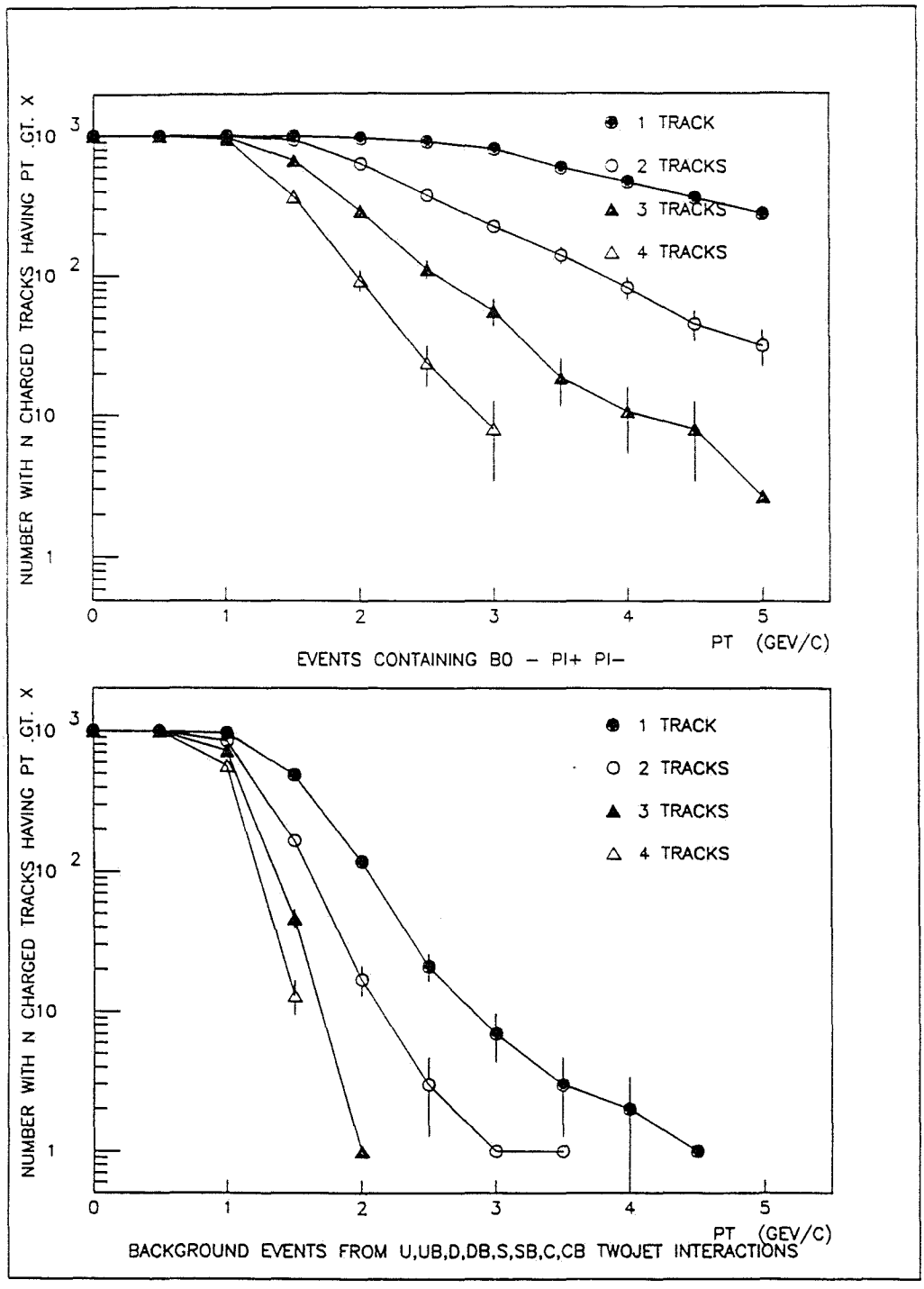

Figure 20: **(a)** The number of charged tracks above a given P_T for events containing a $B \to \pi^+\pi^-$ decay, according to an ISAJET simulation; **(b)** the same for events without any B's.

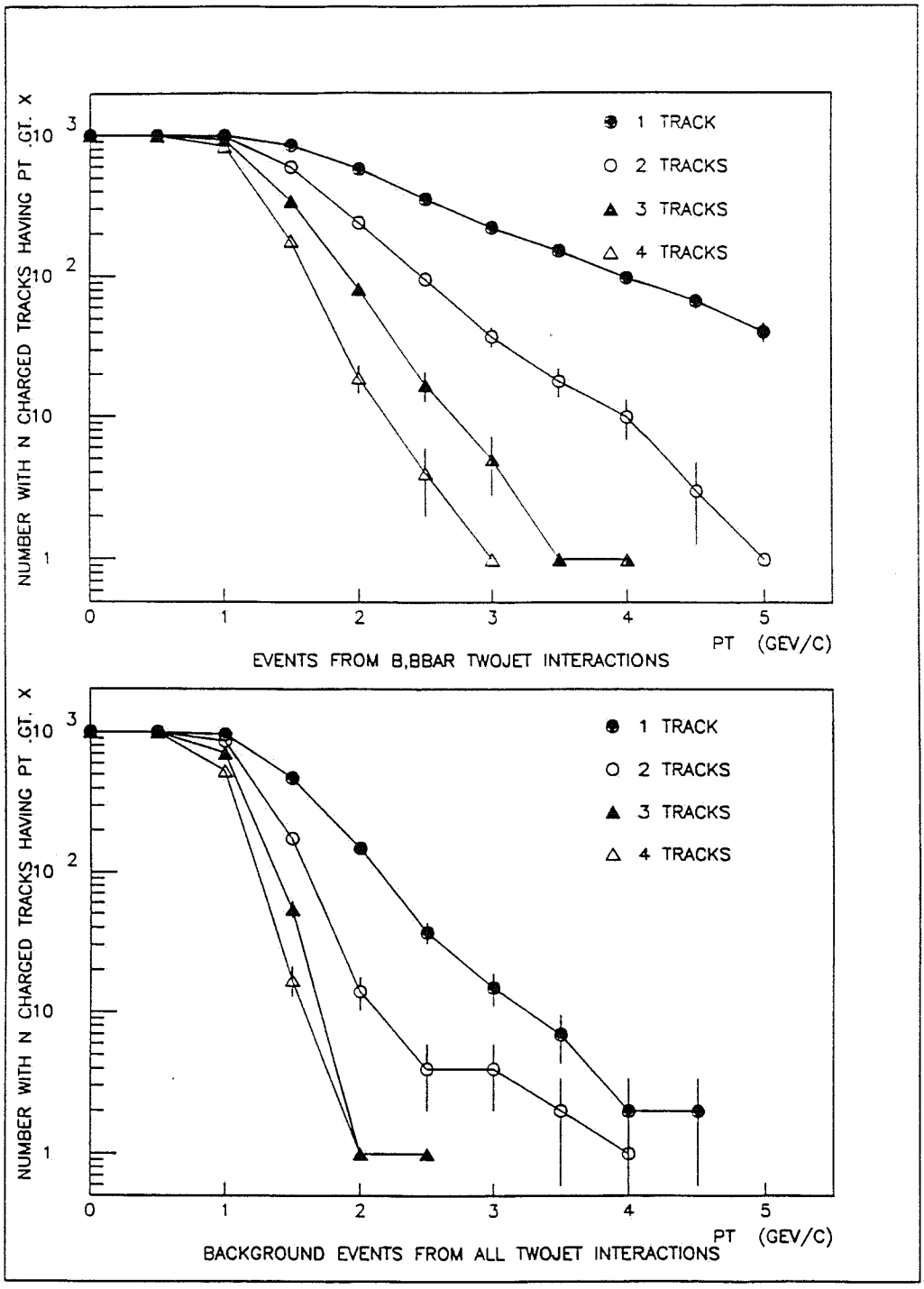

Figure 21: (a) The number of charged tracks above a given P_T for event containing a B decay; (b) the same for all events.

A trigger requiring two tracks both above a P_T cut might be less vulnerable to fake tracks; for a 2-track cut at 2 GeV/c a factor of 50 enhancement can also be obtained, but with only about 70% efficiency for the $B \rightarrow \pi^+\pi^-$ decay, and 30% efficiency for all B decays.

The events surviving the topology trigger are then fed to the processor farm, where an additional factor of 100 reduction in rate is desired. This could be attained if a secondary-vertex-finding algorithm can be implemented online. Simulations of the necessary algorithms on fast numeric processors[35] will be performed in the coming months to evaluate this trigger strategy.

7.2.2 Electron Trigger

Another signature of a B meson which appears suitable as a trigger for the Bottom Collider Detector is a moderate-transverse-momentum electron from a semileptonic decay. As indicated in figure 22 (based on an ISAJET calculation) about 50% of semileptonic B decays yield an electron with $P_T > 1$ GeV/c. The semileptonic branching fraction is 12%, and either B of a $B\bar{B}$ pair is suitable for triggering. Thus a trigger cut of $P_T > 1$ GeV/c on electrons could yield a 12% triggering efficiency for $B\bar{B}$ pairs. If the efficiency of electron identification, including eventual offline reconstruction of a secondary vertex for the $B \rightarrow eX$ decay, is 25% an overall trigger efficiency of 3% could be achieved.

This is a formidable goal at a luminosity of 10^{32} cm^{-2}sec^{-1}, as the electrons must be identified amidst a 5-MHz interaction rate yielding a 500-MHz total rate of particles in the detector. The rate of prompt electrons which would satisfy this trigger is 1-2 kHz.

Only part of the electron trigger could be implemented in the front-end analog logic. The signals from the electromagnetic calorimeter would be combined into candidate clusters. The longitudinal energy distribution within a cluster can provide a rejection factor of over > 100 against charged pions. A pad chamber immediately preceding the calorimeter insures that the cluster is due to a charged particle. Events passing these cuts must be passed into the numeric processors to reject converted photons, Dalitz decays, and $\pi^{\pm}$-π^0 overlaps.

In the rest of this section estimates are given as to the rates of various classes of fake-electron events.

Sources of Electrons

A summary of the rate of electrons from various sources as a function of transverse momentum is shown in figure 22. Prompt electrons derive from direct electronic bottom and charm decay, e^+e^- decays of vector mesons, and Dalitz decays of pseudoscalar mesons. Fake-electron triggers will derive from misidentified $\pi^{\pm}$'s, including $\pi^{\pm}$-π^0 overlaps. A hint of the severity of the fake-electron problem is given

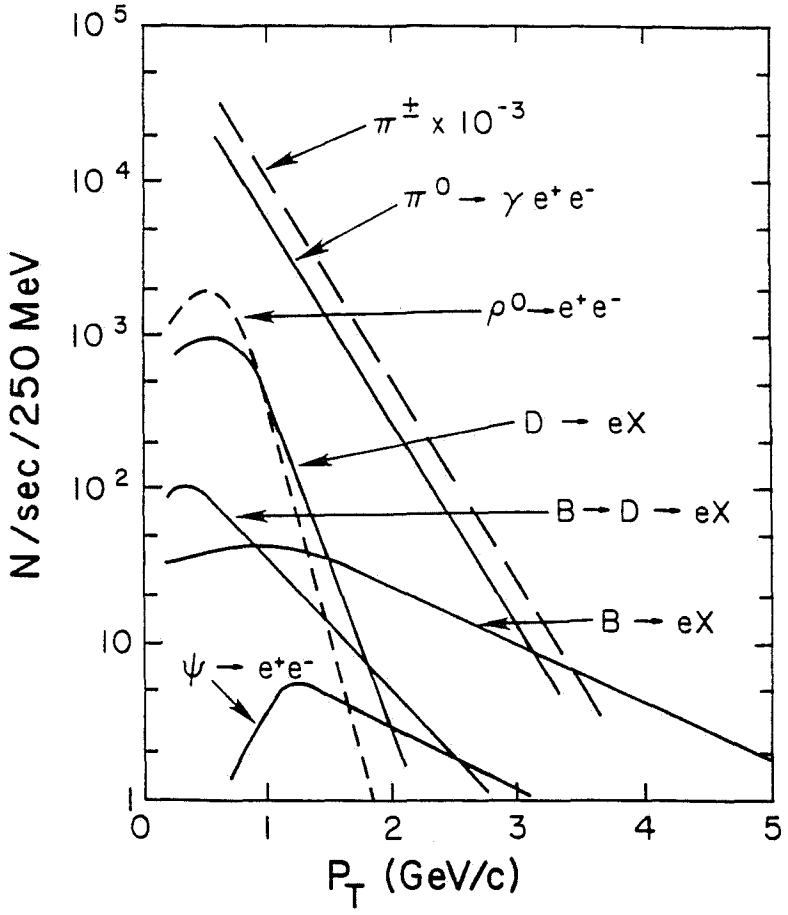

Figure 22: The rate of electrons per 250-MeV/c bin from various sources in p-$\bar{p}$ collisions at $\sqrt{s} = 2$ TeV and luminosity 10^{32} cm^{-2}sec^{-1}.

by the spectrum for $\pi^{\pm}$, also sketched in figure 22.

The present philosophy is to pass all prompt electrons to the offline event-processing stage (supposing the fake-electron triggers can be sufficiently suppressed). With a trigger cut of $P_T > 1$ GeV/c a substantial fraction of the prompt electrons are from B decay, and there is no need to distinguish among the various sources of prompt electrons in the trigger.

Misidentified Hadrons

The rate of charged π's into the detector is about 300 MHz: 60 charged pions per event times the 5-MHz interaction rate. Of these about 15 MHz have transverse momentum above 1 GeV/c and so are potential fake triggers if misidentified as electrons. The online π-e rejection must be greater than 10^4 to reduce fake electron triggers to a 'mere' 1 kHz.

Three types of detectors could contribute to π-e separation: the transition-radiation detectors, the electromagnetic calorimeter, and the RICH counter (at least for low-momentum particles). We suppose that a multi-layer system of tracking

TRD's can yield a rejection factor of 50, but this would be achieved only in the numeric processors. The RICH counter might yield a factor of 5 rejection, most likely also in the numeric processors.

The electromagnetic calorimeter is configured with three longitudinal samples. Comparison of the relative pulse heights in these three layers could yield a factor of 50-100 rejection against pions in a hardware trigger. A match of the shower energy with the charged-track's momentum will be made in the numeric processors; only interactions leading to $\pi^{\pm}$-π^0 charge exchange will survive this E/P cut. The overall rejection factor from the electromagnetic calorimeter is greater than 500. The combined rejection factor from the three detector could then be 10^5, corresponding to a trigger rate of 150/sec from misidentified hadrons.

Overlaps of $\pi^{\pm}$ and γ's from π^0's

A fake-electron trigger is generated if the momentum of a charged pion matches the energy of a π^0 whose shower overlaps the charged-pion track in the electron calorimeter. The TRD and RICH detectors still provide rejection of the charged pion, so the rate of dangerous charged pions is 0.01×15 MHz $= 150$ kHz. Further rejection is obtained by spatially resolving the charged track from the π^0 shower in the electron calorimeter.

A study of the overlap problem was made with the ISAJET Monte Carlo program. Initially, an 'overlap' was defined as a charged pion whose separation from a neutral pion was $|\Delta\eta| < 0.1$ and $|\Delta\phi| < 0.2$. It was found that about 7% of charged pions with $P_T > 1$ GeV/c had such an overlap. These overlaps are dangerous only if the E/P cut is also satisfied. Assuming the electron calorimeter has energy resolution for photons of $\sigma_E = 0.15\sqrt{E}$ the statistical significance of the E/P cut in standard deviations is

$$S.D. = \frac{|E-P|}{0.15\sqrt{E}}.$$

A cut requiring a 2σ separation of E of the π^0 from the P of the $\pi^{\pm}$ yields a rejection factor of 15. The rate of overlaps satisfying the combined trigger cuts is then less than 1 kHz.

The definition of overlap used above is satisfied by a pair of pions whose separation is less than 10 cm at 1-m radius from the beamline. However, two particles should be resolvable in the electron calorimeter if their separation is only 1 cm, which would provide an extra rejection factor of 100. In this case the rate of fake-electron triggers from overlaps would drop to only 10 Hz.

Dalitz decays and γ-Conversions in Matter

The branching fraction for the decay $\pi^0 \rightarrow \gamma e^+ e^-$ is 0.015, as if the vacuum is 0.007 of a radiation length thick. Electrons from conversions of γ's in material will be more numerous than those from Dalitz decay if the photon has traversed

more than 0.007 radiation lengths. For example, with a beam pipe whose wall is 400-μm-thick Be, or 0.001 of a radiation length, photons at angles of less than 1/7 to the beam are more likely to convert in the pipe than during the π^0 decay.

Figure 22 shows that the rate of electrons from Dalitz decay with $P_T > 1$ GeV/c is about 10 kHz at a luminosity of 10^{32} cm^{-2}sec^{-1}. The rate of electrons from γ-conversions in matter will be higher. Thus a rejection factor of order 100 is needed against these conversions.

Conversions outside the beam pipe can be suppressed by fast tracking all the way to the first silicon plane. Conversions in the pipe and Dalitz decays could be suppresed by a dE/dx measurement in the first silicon plane. These factors could only be obtained via algorithms running on the numeric processors.

Electron Detection Efficiency

The process of electron identification inevitably causes some real electrons to be lost. Rough estimates of the various detection efficiencies are:

- Fast tracking: 0.95
- E/P cut: 0.95
- TRD cut: 0.90
- RICH counter cut: 0.95
- Electron shower overlapped by another particle: 0.95
- Photon-conversion cuts: 0.90

The overall efficiency of electron identification might then be 0.62.

7.3 Data Acquisition

7.3.1 Basic Architecture of the Data-Acquisition System

The architecture of the Data Acquisition system takes advantage of several new approaches, in particular:

- Digital transmission via fiber optic cables.
- Numeric processors, especially suited to physics problems, are used for the second-level triggers employing in some cases full reconstruction algorithms.
- Simple barrel shifter for online event building.

A block diagram of the proposed data-acquisition system is shown in Figure 23. Data flow is from top to bottom. Prompt triggers will first reduce the data rate by a factor of 20-50 (subset of detector elements A-Z in figure 23). From this point on in the system there is no other specially built logic for triggering. If the event is accepted by the first-level trigger, fragments are transmitted over fiber-optic cable to the Event-Builder Switch. There can be any number of data sources from each detector element.

The Event-Builder Switch receives event fragments from the detector elements and transmits unformatted total-event streams as its outputs, one total-event stream per output. There are no data-flow bottle necks in this system. Data rates of tens to a few hundreds of GigaBytes/second are possible.

The Receiver/Formatters receive total-event streams, buffer a small number of events, format the data into data structures suitable for higher-level-language applications programs, smooth out data flow and transmit formatted events to banks of processors. A block diagram of an example of a Receiver/Formatter is shown in figure 24.

The Receiver/Formatters pass the data to a farm of numeric processors. Industry-available numeric processors especially suited for solving $AX + B$ problems and capable of 100 Megaflops are used in this farm. Software triggers implemented in these processors reduce the data by a factor of 100-200 permitting the remaining events to be written to tape. These same processors can be used for offline data processing.

More details on the individual components follow.

7.3.2 The Event-Building Process

The Event-Builder Switch is intended to provide the usual event-building function, but at a bandwidth which makes it possible to work with total-event data at an earlier point in the system hierarchy. Together the Transmitters, Receiver/Formatters and the Event-Builder Switch form a communication network which is similar to a standard telephone switching system. Front-end data is buffered in the Transmitters. From there the data is time-division multiplexed on high-speed serial channels through the Event-Builder Switch. Receiver/Formatters at the Switch outputs serve to reassemble and buffer the total-event data.

The Switch is a simple barrel shifter requiring no significant control logic. The serial-line speeds are much higher than is typically used in local telephone systems but lower than in many long-distance trunks. The Transmitters and Receivers/Formatters are basically data buffers with enough control logic to break the data into packets and then reassemble it. Like a telephone network, this system provides a transparent connection from every possible data source to every possible destination with a limited number of wires.

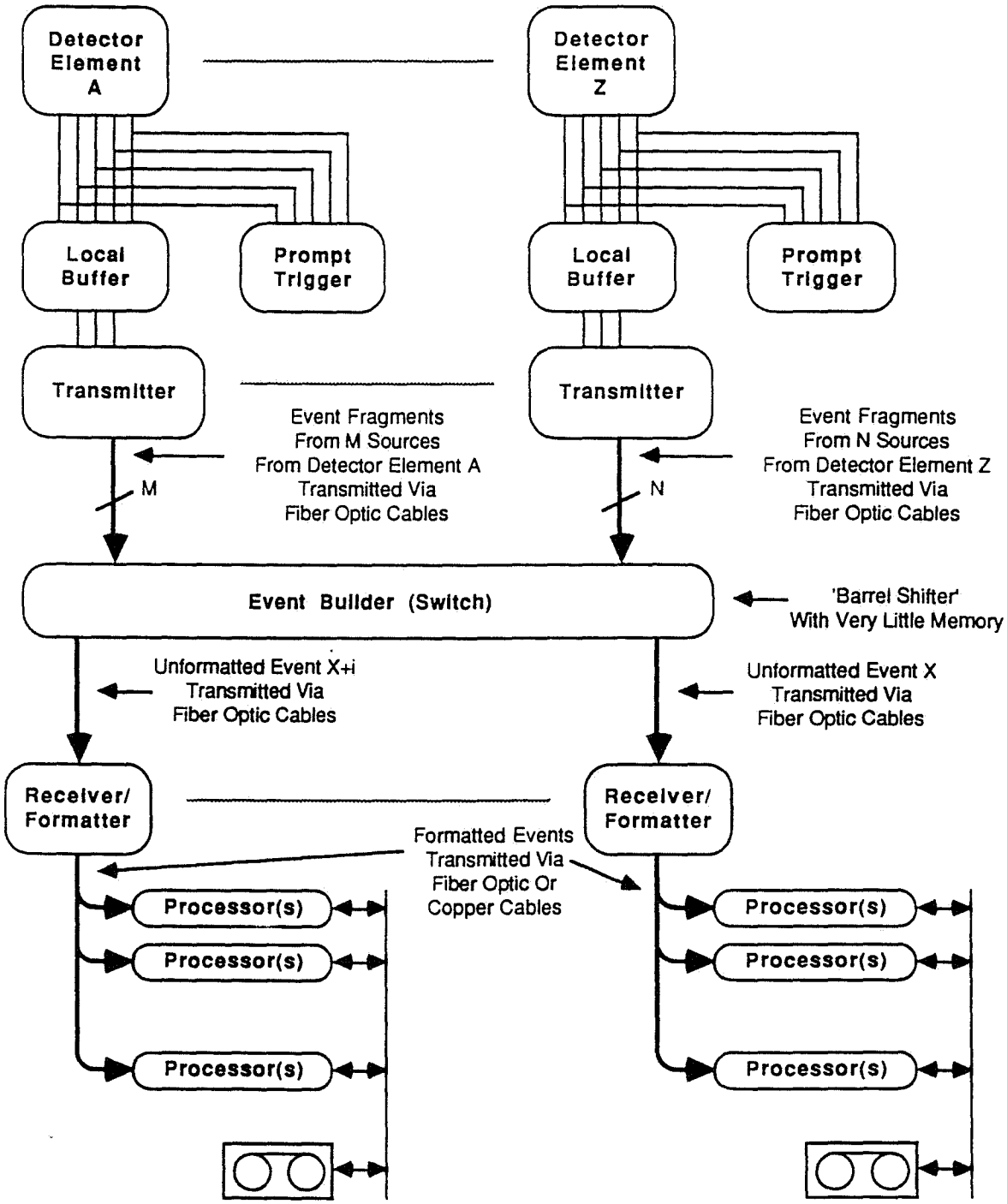

Figure 23: Block diagram of the proposed data-acquisition system.

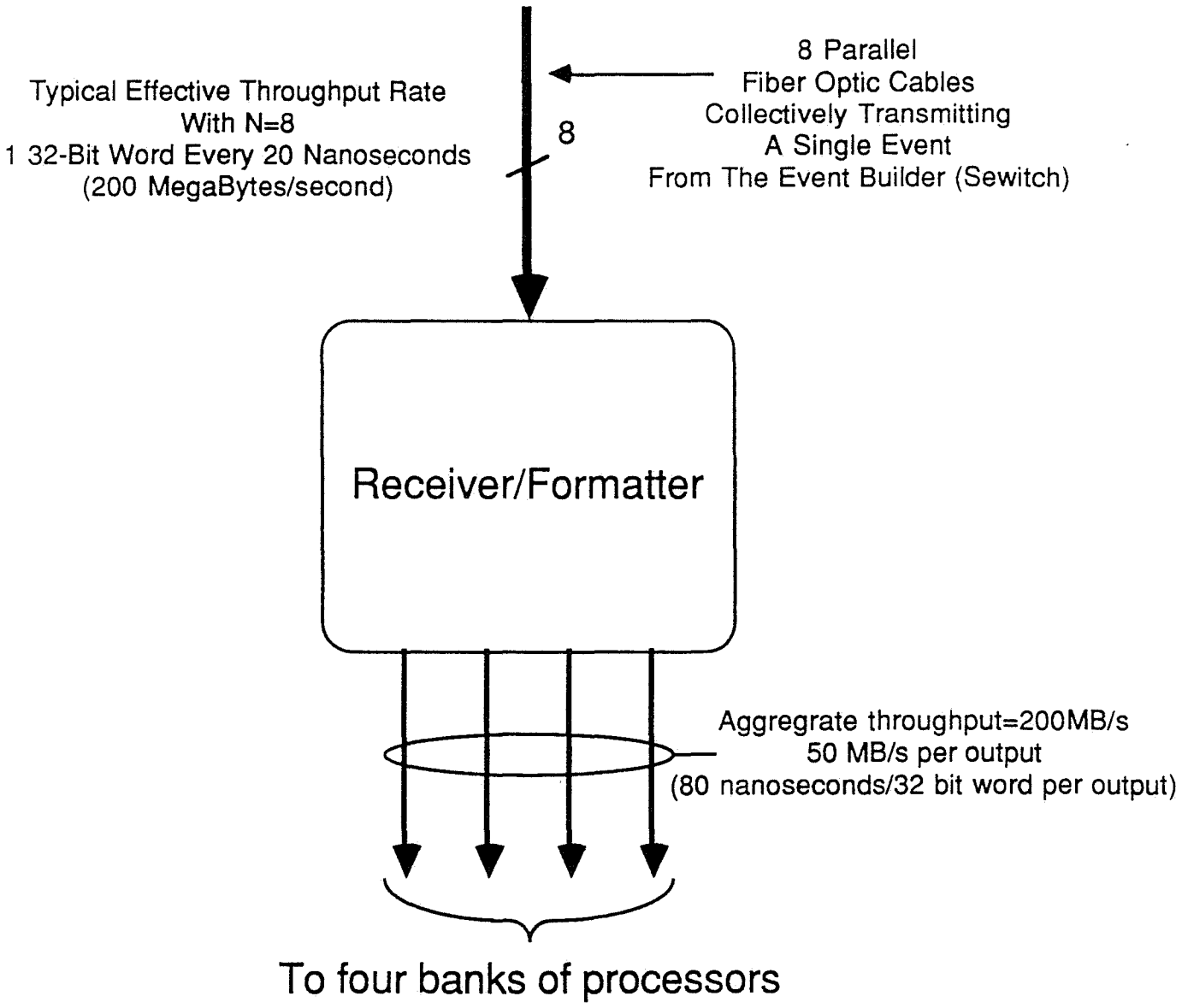

Figure 24: Block diagram of an example implementation of a Receiver/Formatter.

Use of the serial data channels reduces the number of cables leaving the detector while also eliminating many of the synchronization problems associated with parallel busses. It also moves data directly into the processor modules at rates 10 to 20 higher than possible using standard backplanes.

7.3.3 Processors

Microprocessors with on-chip floating point units in the 20 VAX-equivalent range are available now at reasonable cost. Soon-to-be-announced devices will provide an estimated 30 to 35 VAX-equivalents and by 1993 this number will be about 50 VAX-equivalents. We intend to replace much of the specialized electronics used in second-level triggers with programmable processors.

Digital signal processors and RISC processors which have been optimized for graphics applications have many features that would be useful in event reconstruction. For example, these new processors are able to perform fixed- or floating-point $Ax + B$ operations in a single cycle.

7.3.4 Fiber-Optic Digital-Data Transmission

Present fiber-optic data-transmission technology supports rates from less than 1 Megabit per second to higher than 10 Gigabits per second. These rates are achieved by using LED diodes at low frequencies and laser-diode optical transmitters coupled with light-sensitive receiving diodes connected to automatic-gain-controlled amplifiers at high frequencies. Costs vary between \$200 for the slow devices to over \$10,000 per pair for the fast devices.

There are existing communication chips that can be used in an optical-link design. Allowing for transmission overhead, these chips transmit at 12.5 MegaBytes per second. These chips are called TAXI chips and are available from Advanced Micro Devices. These chips accept parallel data, serialize and encode the data, and transmit the data, with the addition of optical components, over fiber-optic cable. At the receiving TAXI chip the data is decoded and converted into parallel form. These rates allow the use of relatively inexpensive LED components. Present estimates are that optical components can be designed for a short link (up to 500 meters) that will cost about \$100 for a transmitter/receiver pair. For single source transmission rates higher than 12.5 MegaBytes per second, several fiber-optic cables can be used in parallel.

8 Machine Issues for Tevatron

8.1 Detector and Collision Hall Issues

The accelerator-related requirements for the Bottom Collider Detector are derived from the performance needed to achieve the physics goals in section 1. The central detector has a dipole magnet with a 1-Tesla field transverse to the beam axis, and a field volume of roughly four by four square meters by four meters along the beam axis. Compensation must be made for the transverse deflection of the beams by the dipole magnet.

The detection of the $B\bar{B}$ decay products requires that a sophisticated solid-state vertex detector and electronics, which may be prone to radiation damage, be located within $1/2''$ of the beamline. There will also be a forward/backward detector that extends several meters up- and downstream from the central detector.

The space required in an experimental hall is roughly determined by the overall dimensions of the detector. As presently envisioned, the detector occupies a volume of about ten by fourteen meters in cross section and 15 meters in length. The dimensions of the spectrometer magnet are comparable to those of the Chicago Cyclotron Magnet but with 4 times larger gap.

There are two ideas for a location for this experiment. The first is to use the $B0$ intersection region. This assumes that CDF no longer occupies this region. The region is ideal for the B collider experiment. The second option is to build a new collision hall, shown in figure 25, that would be available if the proposed Main Ring Injector, part of the Tevatron Upgrade, is constructed. By removing the main ring from the Tevatron tunnel, a third intesection region could be added. Estimates for the cost and downtime are included. The construction for the collision hall will take place during the shutdown for removing the Main Ring Injector and would take 6–10 months.

8.2 Beam Energy

The present detector is designed for the 1×1 TeV beams of the Tevatron. The $B\bar{B}$ production cross section varies approximately linearly with collider beam energy, so an option to run with 1.5-TeV beams would yield 50% more B's at the same luminosity.

8.3 Luminosity

As discussed in section 1, systematic exploration of CP violation in the $B\bar{B}$ system becomes possible for luminosities of order 10^{32} cm^{-2}sec^{-1}. The large investment in the Bottom Collider Detector would be problematic if the average luminosity were

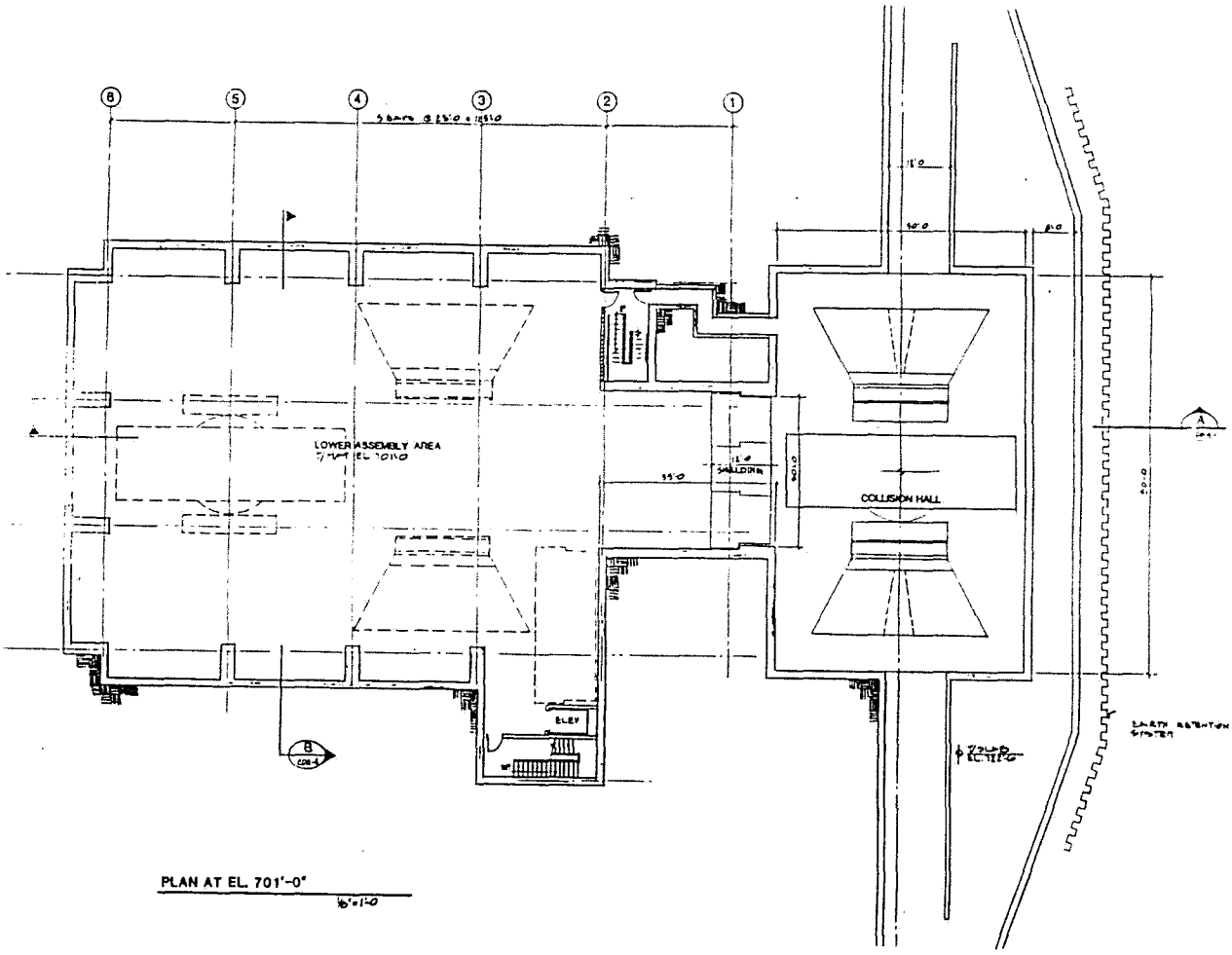

Figure 25: Layout of a new collision hall for the Bottom Collider Detector.

only 10^{30} cm^{-2}sec^{-1}. We recommend an average luminosity of 10^{32}cm^{-2}sec^{-1} be the accelerator goal. The higher luminosity and greater reliability of a p-p collider make this option extremely desirable for B physics.

8.4 Length of the Interaction Region

The length of the interaction region determines the length of the vertex detector. At the present Tevatron the interaction region has a σ of 35 cm. A vertex detector for this region would have to be at least one meter long, with several 10^5 readout channels and unwanted material close to the beam pipe. Current discussions for a Tevatron Upgrade include the possibility of a higher frequency rf system to bunch

the accelerated beam, yielding a shorter interaction region with a σ of 10 cm. The reduction in σ_z would greatly simplify the vertex detector design, lead to a significant reduction in the cost of the vertex detector, and eliminate much undesirable material intercepted by small-angle tracks.

Although all current versions of the Upgrade make provision for a reduced interaction-region length, the p-p option offers the greatest flexibility in that a crossing angle is part of the machine design. By increasing the size of the crossing angle, the length of the interaction region can be proportionately reduced at the expense of luminosity.

8.5 Beam Size

A small transverse beam size is desirable for several reasons. An important signature of B decays is the detection of their decay vertex some few-hundred μm from the primary interaction point. If the beam size is small compared to 100 μm then we gain the considerable advantage of regarding the beam as 1-dimensional. The diameter of the beam pipe, and therefore the vertex detector, is determined by the beam size. The motion of the beams within the beam pipe when the spectrometer dipole is turned on, which also affects the size of the beam pipe, is minimized when the beam size is smallest. And, of course, one achieves higher luminosity with a smaller beam cross section as well.

8.6 Beam Pipe

Conversions of photons in the beam pipe and multiple Coulomb scattering must be minimized in this experiment. A suitable beam pipe could be made of 400-μm-thick beryllium and should be roughly 1/2″ in radius.

8.7 Beam Halo

Halo associated with the beams will contribute to the radiation exposure of the vertex detector and thereby shorten its lifetime. Present data indicate that the silicon detector can survive 10^5 rads and the micro-electronics withstand about 10^4 rads. It is clear that catastrophic beam loss must not occur near the detector. The beam-loss level for abort may need to be lowered compared to present operation.

8.8 Compensation for the Dipole Field

The presence of a spectrometer dipole in the Tevatron would alter the beam trajectory unless compensating measures are taken. The scheme that has been chosen for compensation uses two dogleg bends, one at each end of the straight section and each

20 feet from the center of the interaction region, just downstream of the low-beta quads. The two magnets are both of opposite polarity relative to the spectrometer dipole, and run in series with it (that is, the currents run up together). The spectrometer dipole and compensating magnets are energized only after coasting beam has been established. The beams at the crossing region then move laterally a few mm as the magnets are energized.

8.9 The Detector Hall and Support Facilities

The Detector Hall required for this facility will be comparable in size to that at D0. The detector itself will fill about one half the space available in a straight section at the Tevatron. The compensating dipoles are placed at the outer ends of the straight section. The need for electron detection, calorimetry and particle identification will require the use of special gasses and liquids. The detector may use ethane, TMAE, or TEA. Additional cryogenic support may be necessary to service the main dipole magnet. The detector will require a substantial signal processing area. The Detector Building must also provide for a control room, office and technician space and shop support.

An initial design of a new collision hall has been prepared by Nestander's Engineering Services Group.

8.10 Summary and Status of Accelerator Issues

The broadest issues associated with the accelerator have been successfully worked out. The installation of the spectrometer dipole magnet in the Tevatron seems eminently feasible. The detector size (except perhaps for the magnet yoke) is relatively modest compared to present collider detectors. The magnet parameters are well understood. The location of a vertex detector around the beam pipe is a main feature of this detector and presents special considerations for the accelerator.

The issues that remain to be solved are those that interface with the accelerator beam optics. While the field nonuniformity of the spectrometer dipole is not thought to pose a serious problem it must be studied in more detail. Methods must be developed to insure that a catastrophic loss of beam into the vertex detector does not occur.

Finally, although interesting physics can be performed with an average luminosity of 10^{31} $cm^{-2}sec^{-1}$, the detector will operate at 10^{32} $cm^{-2}sec^{-1}$, and we urge that a concentrated effort be exerted to meet this goal. With this higher luminosity the physics capability will be greatly expanded.

9 Prototyping and Test-Beam Efforts

A Yale/Fermilab group[59] has begun evaluation of the existing VLSI silicon readout chips using a test setup at Fermilab modeled after the one developed for CDF. We have obtained samples of all three available CMOS chips: CAMEX, SVX, and MXI. The noise performance of these chips has typically been evaluated for sampling and readout speeds unique to a particular experiment. Generally, the measurements relevant for the B-detector have not been made. We will measure the levels of signal and noise as a function of sampling rate, readout rate, number of samples, and power dissipation.

Whereas extensive radiation damage measurements have been made for silicon microstrip detectors using intense minimum ionizing beams and neutron sources, the VLSI readout chips have typically been subjected only to radioactive sources for the CMOS chips and synchrotron radiation for the SLAC microplex chip. To study the effect of minimum ionizing radiation we will place the chip directly in a test beam. To study the effect of heavy ionizing radiation we will place the readout chip downstream of various targets of substantial interaction and radiation lengths. This will be a realistic test of "albedo" encountered in a collider experiment from interactions in the beam pipe and detector material. We will make these measurements over a broad range of beam energies to simulate those encountered in colliding beam interactions.

A key feature of these measurements will be use of readout chips wire bonded to a silicon microstrip dectector to enable evaluation of the *system performance* and not just the readout chip alone. Thus the problems of channel-to-channel variation, RF shielding, cooling, and mechanical mounting will be addressed. In addition, we will develop the practical expertise necessary to mount an experiment with these devices.

Other prototyping efforts associated with this proposal include evaluations of double-sided silicon detectors at the U. of Oklahoma,[60] studies of scintillating fibers for forward tracking and/or calorimetry at Northeastern U., studies of silicon drift chambers at Princeton U.,[61] and studies of new-technology numeric processors at Fermilab and U. Penn.[35]

10 Cost

The estimated costs are quoted in thousands of dollars. Items 4-8 are for mechanical components of the detectors; the cost of the front-end electronics is quoted separately.

1. Magnet

   New magnet coils 3,000
   or, use MFTF coils 500
   Cryogenics 2,000
   Iron 1,500
   Assembly 1,000

2. Be Beam pipe 200

3. Compensating magnets 200

4. Silicon vertex detector

   400 wafers @ \$1k/wafer 400
   Engineering: 4 FTE's $\times$ 2 years @ 60k 480

5. Straw-tube chambers

   2×10^5 channels @ \$2 per straw 400
   Engineering: 3 FTE's $\times$ 2 years @ 60k 360
   Test equipment 100

6. TRD 1,000

7. RICH 3,000

8. EM calorimeter 3,000

9. Time-of-Flight Counters 200

10. Prompt trigger 400

11. Data acquisition

    Processor farm 3,200
    100 Exabyte tape drives 400

Host VAX, disk drives and workstations.....1,000

Engineering: 8 FTE's × 3 years @ 75k.....1,800

6 FTE's × 3 years @ 50k.....900

12. Front-end electronics

Silicon vertex detector: 500k channels @ $1.....500

Straw-tubes: 2×10^5 @ $6 per channel.....1,200

TRD: 10^6 pads @ $1 per channel.....1,000

RICH: 10^6 pads @ $1 per channel.....1,000

EM calorimeter: 50k channels @ $6.....300

13. Chip development

6 analog chips: each 1 FTE × 2 years @ 75k.....900

Foundry costs: 6 chips × 2 runs × 25k.....300

3 digital chips: 2 runs × 40k.....240

Test equipment.....500

Total.....27,980

Acknowledgements

We thank the laboratory management, Leon Lederman, John Peoples, Helen Edwards and Ken Stanfield for general support in this continuing effort. James Bjorken has continuously stressed the importance of bottom physics for several years now, and has contributed greatly to our enthusiasm and understanding of this subject. We also thank Bob Wands, Alan Wehmann, Ron Fast and Thorton Murphy for help with the beginnings of a magnet design. Finally we thank Rick Van Berg for help with the Front End Electronics section and Wayne Nestander for help with the collision hall study.

11 References

[1] P. Karchin, N. S. Lockyer, *et al.*, *Proposal for a Bottom Collider Detector* **BCD**, (March 1987).

[2] N. Reay, *et al.*, *Letter of Intent for a Tevatron Beauty Factory*, (March 1987).

[3] N. S. Lockyer, *Issues for a Bottom Collider Detector at Fermilab*, Proceedings of the High Sensitivity Beauty Physics Workshop held at Fermilab (Nov. 1987), Editors. J. Slaughter, N. S. Lockyer, M. Schmidt.

[4] Neville W. Reay *et al.*, *Summary of the Collider Architecture Working Group*, Proceedings of the High Sensitivity Beauty Physics Workshop held at Fermilab (Nov. 1987).

[5] K. Foley *et al.*, *A Beauty Spectrometer for the SSC*, Proceedings of the Workshop on Experiments, Detectors and Experimental Areas for the Supercollider, (Berkeley 1987) R. Donaldson and G. Gilchriese editors.

[6] BCD Study Group, *Status Report of the Fermilab B Collider Study Group*, Princeton University preprint DOE/ER/3072-45 (June 1988).

[7] E. Berger, *Benchmark Cross Sections for Bottom Quark Production*, Proceedings of the High Sensitivity Beauty Physics Workshop held at Fermilab (Nov. 1987); and private communication, Ed Berger.

[8] E. Berger, *Heavy Flavor Production*, ANL-HEP-PR 88-26

[9] P.Nason, S. Dawson, R.K. Ellis, *The total cross section for the production of heavy quarks in hadronic collisions*, Fermilab 87-222-T; and private communication, Keith Ellis.

[10] M. Schmidt, J. L. Rosner, A. I. Sanda, *Physics Group Summary*, Proceedings of the High Sensitivity Beauty Physics Workshop held at Fermilab (Nov. 1987).

[11] I. I. Bigi and A. I. Sanda, *CP Violation in Heavy Flavor Decays*, Nucl. Phys. **B281** (1987) 41-71.

[12] F. Gilman, *B Physics*, to appear in the proceedings of Les Rencontres de Physique de la Vallee d'Aoste (La Thuile, Italy, Feb. 1988).

[13] H. Harari, *B Physics*, to appear in the Proceedings of Les Rencontres de Physique de la Vallee d'Aoste (La Thuile, Italy, Feb. 1988).

[14] C. Hamzaoui, J. L. Rosner, A. I. Sanda, *B Meson Decay Asymmetry and $B\bar{B}$ Mixing*, Proceedings of the High Sensitivity Beauty Physics Workshop held at Fermilab (Nov. 1987).

[15] K.J. Foley *et al.*, *Bottom and Top Physics*, Proceedings of the Workshop on Experiments, Detectors and Experimental Areas for the SSC (Berkeley, 1987).

[16] I. Dunietz, *Measurement of the Mass and Lifetime Differences between the Heavy and Light B_s Eigenstates*, Proceedings of the High Sensitivity Beauty Physics Workshop held at Fermilab (Nov. 1987).

[17] I. I. Bigi and B. Stech, *Future Lessons from Two-Prong Two Body decays of Beauty*, Proceedings of the High Sensitivity Beauty Physics Workshop held at Fermilab (Nov. 1987).

[18] Ling-Lie Chau and Hai-Yang Cheng, *In Search of V_{ub} in Nonleptonic Decays from the Quark Diagram Scheme*, Physics Letters **B197** (1987).

[19] A. Soni. and G. Hou, *Loop Induced Rare B Decays*, Proceedings of the U.C.L.A. Workshop, Linear Collider $B\bar{B}$ Factory Conceptual Design, Editor Donald Stork (Jan. 1987).

[20] A. Ali, *$B\bar{B}$ Mixing - A Reappraisal*, Proceedings of the U.C.L.A. Workshop, Linear Collider $B\bar{B}$ Factory Conceptual Design, Editor Donald Stork (Jan. 1987).

[21] H. Albrecht *et al.*, (Argus Collaboration), Phys. Lett. **B192** (1987) 245.

[22] J. Bjorken, *Prospects for Future Fixed-Target B Physics at Fermilab*, Proceedings of the High Sensitivity Beauty Physics Workshop held at Fermilab (Nov. 1987).

[23] J. Sandweiss and B. Cox, *Summary of Fixed Target Working Group*, Proceedings of the High Sensitivity Beauty Physics Workshop held at Fermilab (Nov. 1987).

[24] P. Garbincius, *Review of Fixed-Target B Physics at Fermilab*, Proceedings of the High Sensitivity Beauty Physics Workshop held at Fermilab (Nov. 1987).

[25] F. Olness and W.-K. Tung, *Small-x Physics at the SSC and the Tevatron*, Int. Jour. Mod. Phys. **A2** (1987) 1413.

[26] A. J. Lankford and M. Johnson, *et al.*, *Summary of the Trigger and Data Acquisition Group*, Proceedings of the High Sensitivity Beauty Physics Workshop held at Fermilab (Nov. 1987).

[27] E.Barsotti,M.Bowden,H. Gonzalez, and C. Swoboda, *Digital Triggers & Data Acquisition Using New Microplex & Data Compaction ICs. Many Parallel Math Processors, & Fiber Optics to Fast Digital Triggers & Higher Level Farms*, Proceedings of the Workshop on High Sensitivity Beauty Physics at Fermilab (Nov. 11-14, 1987) Editors. J. Slaughter, N. S. Lockyer, M.Schmidt.

[28] R. Van Berg, *Front-End Architectures for New Beauty Detectors*, Proceedings of the High Sensitivity Beauty Physics Workshop held at Fermilab (Nov. 1987).

[29] V. Ashford *et al.*, *RICH for SLD*, IEEE Trans Nucl. Sci. **NS-34** (1987) 499.

[30] J. Sequinot, *RICH for DELPHI*, Second Hellinic School on Elementary Particle Physics, 61 (1985).

[31] G. Bassompierre, *et al.*, *JETSET Proposal*, CERN PSCC86-23 This is an effort to trigger on a Liquid Rich Counter in LEAR. We have talked to Y. Onel and J. Kirkby and will continue dialog in the future.

[32] O. Botner, *et al.*, Nucl. Instr and Meth. **A257** (1987) 580.

[33] G. Hallewell, *et al.*, *Progress Report on the SLD Cerenkov Ring Imaging Detector System*, SLAC-PUB-4405 (September, 1987).

[34] P. Beltran, *et al.*, *Design of the Forward RICH counter in DELPHI and Results from the Operation of a Full-Scale Prototype*, CERN-EP/88-80 (1 July 1988).

[35] N. Lockyer, *et al.*, *Proposal for Generic Detector R&D for the SSC*, (September, 1988).

[36] T. Ypsilantis, *RICH/CRID for Future Hadron Collider Experiments*, Talk given at Snowmass '88 (July, 1988).

[37] J Va'Vra, IEEE Trans. Nucl. Scvi. **NS-34** (1987) 486.

[38] T. Ludlam, *Summary of the Particle Identification Group*, Proceedings of the High Sensitivity Beauty Physics Workshop held at Fermilab (Nov. 1987).

[39] M. Strovinck, D0 Collaboration Internal Note.

[40] U. Amaldi and G. Coignet, *Conceptual Design of A Multipurpose Beauty Factory Based on Superconducting Cavities*, CERN-EP/86-211 (Dec. 16, 1986).

[41] D. Cline, *Conceptual Design for a High Luminosity Linear Collider $B\bar{B}$ Factory*, Proceedings of the U.C.L.A. Workshop, Linear Collider $B\bar{B}$ Factory Conceptual Design, Editor Donald Stork (Jan. 1987).

[42] R. Eichler, T. Nakada, K. R. Schubert, S. Weseler, and K. Wille, *Proposal for a Double Storage Ring*, SIN Report PR-86-13 (Nov. 1986).

[43] H. Aihara, *B Factory at KEK*, Proceedings of the U.C.L.A. Workshop, Linear Collider $B\bar{B}$ Factory Conceptual Design, Editor Donald Stork (Jan. 1987).

[44] E. Bloom, *N-PEP $B\bar{B}$ Factory*, Proceedings of the U.C.L.A. Workshop, Linear Collider $B\bar{B}$ Factory Conceptual Design, Editor Donald Stork (Jan. 1987),

[45] F. Paige and S. Protopopescu, *Isajet Monte Carlo.*

[46] P. Holl *et al.*, *Strip Detectors with Capacitive Readout and a New Method of Integrated Bias Coupling*, Contributed paper to the XXIV International Conference on High Energy Physics (Munich, Aug. 4-10, 1988).

[47] T. Kondo, *Radiation Damage of Silicon Devices*, from Future Directions in Detector Research and Development for Experiments at PP Colliders (Snowmass, Colorado, July 5-7, 1988).

[48] G. Lutz *et al.*, *Low Noise Monolithic CMOS Front End Electronics*, Nucl. Instr. Meth. **A263** (1988) 163-173.

[49] W. Buttler *et al.*, *Noise Performance and Radiation Hardness of the CAMEX64 Analog Multiplexing Readout Chip*, Contribution to the XXIV International Conference on High Energy Physics (M,unich, August, 1988).

[50] S. Kleinfelder *et al.*, *A Flexible 128 Channel Silicon Strip Detector Instrumentation Integrated Circuit with Sparse Data Readout*, IEEE 1987 Nucl. Sci. Symposiu, (San Francisco).

[51] P.P. Allport, P. Seller and M. Tyndal, *A Low Power CMOS VLSI Multiplexed Amplifier for Silicon Strip Detectors*, London Conference on Position Sensitive Detectors (Sept., 1987).

[52] J. T. Walker *et al.*, *Development of High Density Readout for Diode Strip Detectors*, Nucl. Instr. Meth. **226** (1984) 200.

[53] S.K. Dhawan *et al.*, *A RICH MWPC Pad Readout by Using Custom Microplex I.C.*, IEEE Trans. Nucl. Sci. 35 (1988) 436.

[54] P. Baringer et al., Nuc. Instr. and Meth. **A254** (1987) 542.

[55] S.L. Shapiro *et al.*, *Silicon PIN Diode Array Hybrids for Charged Particle Detectors*, SLAC-PUB-4701 (September 1988).

[56] R. DeSalvo, *A Proposal for an SSC Central Tracking Detector*, Cornell University preprint CLNS87/52 (1987).

[57] R. Thun, *Prospects for Wire Chambers at High Luminosity*, presented at Future Directions in Detector R&D for Experiments at pp Colliders (Snowmass, 1988).

[58] D. Groom, *Radiation Levels in SSC Experiments*, presented at Future Directions in Detector R&D for Experiments at pp Colliders (Snowmass, 1988).

[59] S.K. Dhawan *et al.*, *Performance Limits of Silicon Strip Front-End Electronics for the SSC B Detector*, Yale U. proposal for SSC Detector Development (1988).

[60] G.R. Kalbfleisch and P. Skubic, *Considerations Regarding Double-Sided Solid State Detectors*, U. Of Oklahoma preprint (Feb. 1988); G.R. Kalbfleisch, P.L. Skubic and M.A. Lambrecht, *Results on Signal Correlations from a 'Micron' Doubled-Sided Mini-Strip Detector*, U. of Oklahoma preprint (Aug. 1988).

[61] K.T. McDonald and M.V. Purohit, *Proposal for Generic Detector Development*, Princeton U. preprint DOE/ER/3072-46 (Aug. 1988).